FLEXURAL PERFORMANCE OF CONCRETE BEAMS STRENGTHENED USING CFRP SHEETS WITH LARGE SPIKE ANCHORS

by

Maha A. Assad

A Thesis Proposal Presented to the Faculty of the
American University of Sharjah
College of Engineering
in Partial Fulfillment
of the Requirements
for the Degree of

Master of Science in
Civil Engineering

Sharjah, United Arab Emirates

March 2023

Declaration of Authorship

I declare that this thesis is my own work and, to the best of my knowledge and belief, it does not contain material published or written by a third party, except where permission has been obtained and/or appropriately cited through full and accurate referencing.

Signature …….…… Maha Assad……

Date ……..…….……16/03/2023……

Approvals

We, the undersigned, approve the Masters Thesis written by: Maha Assad

Thesis Title: Flexural Performance of Concrete Beams

Strengthened Using CFRP Sheets with Large Spike Anchors

Date of Defense: 16/03/2023

Name, Title and Affiliation	**Signature**
Dr. Rami Haweeleh Professor Department of Civil Engineering Thesis Advisor	
Dr. Jamal Abdalla Professor Department of Civil Engineering Thesis Co-Advisor	
Dr. Farid Abed Professor Department of Civil Engineering Thesis Committee Member	
Dr. Wael Abuzaid Associate Professor Department of Mechanical Engineering University Name: American University of Sharjah Thesis Examiner (External)	

Accepted by:

Dr. Fadi Aloul
Dean
College/School of Engineering

Dr. Mohamed El-Tarhuni
Vice Provost for Research and Graduate Studies
Office of Research and Graduate Studies

Acknowledgements

I would like to express my gratitude to my supervisors, Dr. Rami Hawileh and Dr. Jamal Abdalla, for their guidance and support throughout my research journey. I am also grateful to my thesis committee, Dr. Farid Abed and Dr. Wael Abuzaid for their invaluable insights, constructive feedback, and their effort in reviewing this research. I extend my appreciation to the American University of Sharjah for granting me graduate teaching and research assistantship. In addition, I want to recognize the assistance provided by AUS research grant FRG22-C, which was crucial in the completion of this research endeavor. Furthermore, I am grateful to Engineers Haya Mhanna, Arshi Faridi, Ahmed Selim, and Mohammad Ansari for their invaluable aid in the laboratory work.

I also would like to thank Structural Technologies LLC. for providing the materials and labor to prepare the test specimens. A special thanks goes to Dr. Tarek Alkhrdaji in Structural Technologies LLC. for his guidance which helped a lot in establishing the test matrix of the study.

Lastly, I would like to convey my heartfelt gratitude to my life partner, Emad, for providing unwavering emotional support and encouragement throughout this process. I am also deeply grateful to my beloved family for their contributions and support.

Dedication

To the pure souls of those who passed away in defence of the beloved Palestine, you lightened our path to freedom and liberation…

Abstract

Fiber-reinforced polymers (FRP) have a proven strength enhancement capability when attached to reinforced concrete (RC) beams. However, the inherent brittleness of FRP composites largely sacrifices the full load-carrying capacity of externally bonded FRP strengthening systems. The use of carbon fiber-reinforced polymers (CFRP) splay anchors has demonstrated positive outcomes in terms of enhancing the capacity of strengthened members and mitigating debonding. Limited research studies have been carried out to examine the effect of CFRP splay anchor parameters on the flexural behavior of RC beams anchored with small diameter anchors. The aim of this study is to examine the effect of large anchors, specifically, anchors with a diameter of more than 14 mm. Accordingly, a total of seventeen beams were cast and tested under four-point bending test. Fifteen beams were strengthened using CFRP sheets and anchored with different configurations of CFRP spike anchors. The investigated variables in the experimental program are anchor's dowel diameter, embedment depth, fan length, insertion angle, and number of anchors. Test results of the anchored specimens in terms of load-deflection responses, failure modes, strain in the concrete, steel reinforcement, and CFRP laminates were compared to that of the control unstrengthened and unanchored strengthened specimens. The test results indicate that CFRP anchors enhanced the strength of the CFRP laminates by 12-53% over the unanchored specimens. It was observed that larger diameter anchors provided a considerably improved strength enhancement compared to smaller diameter anchors, on average by 28%. It was also concluded that bonding CFRP laminates by well-designed CFRP anchors highly utilized the strain attained in CFRP laminates. In addition, the flexural strength of the anchored beams is predicted using the ACI440.2R-17, CSA-S806.12(R2017), and *fib*-14 design guidelines. Based on comparison with the experimental results, the ACI440.2R-17 and *fib*-14 provisions provided reasonable predictions according to the debonding/delamination equation and assuming no fully bonded action is developed due to anchorage.

Keywords: Externally Bonded Reinforcement (EBR); Carbon Fiber Reinforced Polymer (CFRP); RC beams; CFRP splay anchors; flexure.

Table of Contents

Abstract 6

List of Figures 10

List of Tables 13

Chapter 1. Introduction 14

1.1. Overview 14

1.2. Research Significance 18

1.3. Research Objectives 20

Chapter 2. Literature Review 21

2.1. Flexural Strengthening of Concrete Beams with FRP Laminates 21

2.2. Interface Behavior between CFRP and Concrete 22

2.3. Previous Tests Conducted on CFRP Anchors 23

2.3.1. Pullout tests 23

2.3.2. Single shear tests 26

2.3.3. Bending tests 27

2.4. Flexural Capacity Predictions of FRP-Strengthened RC Beams 30

2.4.1. American concrete institute design guidelines for flexural strength (ACI 440.2R-17) [53] 30

2.4.2. Canadian standards association CSA-S806.12 (R 2017) [59] 35

2.4.3. International federation for structural concrete (fib) bulletin 90 (2019) [60] 35

Chapter 3. Experimental Program 38

3.1. Specimen Details 38

3.2. Material Properties 40

3.2.1. Concrete. 40

3.2.2. Steel reinforcement 41

3.2.3. CFRP sheets and epoxy. 42

3.3. Test Matrix 43
3.4. Test Setup 45
3.5. Preparation and Strengthening of Specimens 46
3.5.1. Preparation of RC beams 46
3.5.2. Strengthening of specimens 47
Chapter 4. Experimental Program 52
4.1. Failure Modes 52
4.2. Strain in Flexural Steel Reinforcement and Concrete 61
4.3. Load-Deflection Curves 66
4.4. Strain measurements in the CFRP laminates 70
Chapter 5. Discussion of Results 75
5.1. Flexural Strength 75
5.1.1. Effect of strengthening 75
5.1.2. Effect of anchorage 75
5.1.3. Effect of anchor dowel diameter 77
5.1.4. Effect of embedment depth 78
5.1.5. Effect of fan length 80
5.1.6. Effect of insertion angle 81
5.1.7. Effect of the number of anchors 81
5.1.8. Effect of anchor's area to sheet's area ratio (ASR) 82
5.2. Ductility 83
Chapter 6. Analytical Predictions 86
6.1. Flexural Strength 86
6.2. Strain in the CFRP laminates at failure 88
Chapter 7. Summary and Conclusions 93
7.1. Summary 93
7.2. Conclusions 93
7.3. Suggested Future Research work 95
References 96

Vita.....101

List of Figures

Figure 1: Elements of FRP spike anchors [14] 17
Figure 2: Applications of straight anchors and bent FRP anchors 17
Figure 3: Failure modes of FRP spike anchors [16] 18
Figure 4: Debonding failure modes mechanism [40] 23
Figure 5: Effect of embedment depth on the pullout capacity of FRP anchors [20] ... 24
Figure 6: Test setup in Castillo et al. [22] 26
Figure 7: Finite element model components in [47] 27
Figure 8: Proposed method of anchorage [50] 29
Figure 9: Schematic of the RC beam (dimensions in mm) 38
Figure 10: Strengthening and anchor detailing of the beams with: (a) FRP laminate; (b) FRP laminate with two anchors; (c) FRP laminate with four anchors; (d) FRP laminate with inclined anchors 39
Figure 11: Bottom view of strengthened beam specimens with: (a) FRP laminate; (b) FRP laminate and two anchors; (c) FRP laminate and four anchors 40
Figure 12: Compressive strength testing machine 41
Figure 13: Failure of concrete samples 41
Figure 14: Tensile strength test of steel bars 42
Figure 15: Schematic of the test setup 46
Figure 16: Test setup 46
Figure 17: Casting of specimens 47
Figure 18: Strengthening procedure 48
Figure 19: Anchors installation 50
Figure 20: Strengthened and anchored specimens 51
Figure 21: Failure mode of group 1 beams 54
Figure 22: Failure mode of group 2 beams 55
Figure 23: Failure mode of group 3 beams 56
Figure 24: Failure mode of group 4 beams 57
Figure 25: Failure mode of group 5 beams 59
Figure 26: Failure mode of group 6 beams 60

Figure 27: Failure modes of group 7 beams 61
Figure 28: Strain measurements of concrete and steel for Group 1 beams 62
Figure 29: Strain measurements of concrete and steel for Group 2 beams 63
Figure 30: Strain measurements of concrete and steel for Group 3 beams 63
Figure 31: Strain measurements of concrete and steel for Group 4 beams 64
Figure 32: Strain measurements of concrete and steel for Group 5 beams 65
Figure 33: Strain measurements of concrete and steel for Group 6 beams 66
Figure 34: Strain measurements of concrete and steel for Group 7 beams 66
Figure 35: load-deflection curve for Group 2 specimens 67
Figure 36: Load-deflection curve for Group 3 specimens 68
Figure 37: Load-deflection curve for Group 4 specimens 69
Figure 38: Load-deflection curve for Group 5 specimens 70
Figure 39: Load-deflection curve for Group 6 specimens 70
Figure 40: Load-deflection curve for Group 7 specimens 70
Figure 41: Load-strain curves of all strengthened specimens.....71
Figure 42: Load-strain curves of CFRP for Group 2 specimens 72
Figure 43: Load-strain curves of CFRP for Group 3 specimens 72
Figure 44: Load-strain curves of CFRP for Group 4 specimens 73
Figure 45: Load-strain curves of CFRP for Group 5 specimens 73
Figure 46: Load-strain curves of CFRP for Group 6 specimens 74
Figure 47: Load-strain curves of CFRP for Group 7 specimens 74
Figure 48: Percentage increase in ultimate load for the tested specimens.....77
Figure 49: Percentage of strain utilization 77
Figure 50: Effect of embedment depth for different groups 79
Figure 51: Effect of embedment depth 79
Figure 52: Effect of fan length in different groups 80
Figure 53: Effect of fan length.....81
Figure 54: Effect of insertion angle 82
Figure 55: Effect of ASR ratio.....83
Figure 56: Ductility index for all specimens.....85
Figure 57: Percentage decrease in ductiltiy index below B 85
Figure 58: Comparison between the experimental and predicted flexural strength 87

Figure 59: Comparison of ultimate strain to calculated debonding strain from previous models 90
Figure 60: Comparison of $\varepsilon_{ult}/\varepsilon_{deb}$ from different codes according to the diameter 92

List of Tables

Table 1: Concrete compressive strength results.....40
Table 2: Mechanical properties of steel bars 42
Table 3: Properties of dry CFRP sheets and anchors, CFRP laminates (sheets with epoxy), and epoxy adhesive 43
Table 4: Test matrix 45
Table 5: Summary of failure modes.....52
Table 6: Summary of the test results.....76
Table 7: Deflection values and ductiltiy results.....84
Table 8: Comparison between predicted and experimental flexural strength.....87
Table 9: Calculated strain values from previous models 88

Chapter 1. Introduction

1.1. Overview

Strengthening and retrofitting of existing structures has been an outstanding solution to overcome the consequences of several actions that lead to the deterioration of structural members [1], [2]. Namely, exposure to severe environmental conditions, excessive loading due to change in structure's usage, and design or construction flaws. The use of fiber reinforced polymers (FRP) as a strengthening system has received widespread acceptance in the last four decades. The efficacy of such strengthening system results from the high strength it offers compared to its weight, the durability of the FRP materials, obtrusiveness, and versatility [3]. Because of these preferences, it is considered a superlative strengthening strategy when compared to traditional systems, such as steel plates, section enlargement, and concrete jacketing.

FRP composite materials consists of high strength continuous fibers embedded in a polymer matrix. The conventional fibers include carbon (CFRP), glass (GFRP), and aramid (AFRP). They have been proven successful to enhance the properties of all basic structural components. For instance, axial, flexure, and shear load capacities, ductility, fatigue life, and serviceability. The typical densities of FRP range from 1.2 g/cm^3 to 2.1 g/cm^3 which is 4-6 times larger than that of steel. Conventional FRP composites exhibit a linear elastic behavior and provide stiffness and strength in tension along the fiber's direction until rupture at low elastic strains; typically, 1-2% [2]–[4].

FRPs can be applied in several forms to enhance the capacity of reinforced concrete (RC) members. The most common and effective strengthening techniques of RC beams in flexure include applying externally bonded reinforcement (EBR) to the concrete surface or inserting near-surface mounted (NSM) FRP rods in the tension side of the beam [3]. In external bonding, FRP sheets are bonded to the concrete surfaces via epoxy adhesives by the wet-layup process. Many studies have shown the effectiveness of this method in enhancing the flexural capacity of RC beams [5], [6]. The externally bonded FRP laminates are attached to the tension face of the concrete member where the fibers are oriented along the longitudinal axis of the beam. This

strengthening technique has been known as a widely accepted retrofitting solution in the structural engineering community.

The major disadvantage of externally bonded FRP laminates strengthening system is the premature debonding of the FRP from the concrete substrate [7]. This type of failure prevents the FRP composite from reaching its ultimate strength. Given that these materials behave in a linear elastic manner up to rupture at very low strains, the debonding strain at which the FRP sheet is separated from concrete is even lower (less than 1%) [8]. The detachment of the FRP from the concrete surface is the dominant failure mode for EBR systems and is considered a brittle failure mode since it occurs suddenly before the member utilizes its full expected strength.

One of the reasons for the debonding failure is the development of stresses between FRP and concrete at the onset of cracking in the maximum moment region [7]. The flexural and/ or flexural-shear cracks progress throughout the length of the FRP and the binding matrix which results in stress concentrations at the interface between the FRP and concrete. The concrete cover separation is also another form of debonding failure which is called delamination [9]. It occurs when the FRP laminate detaches from the concrete with the adhered concrete cover due to stress concentration at the sheet tip. The crack that initiates at an angle, changes to a horizontal crack at the level of primary steel reinforcement. Debonding should be avoided and prevented in RC beams where a ductile mode of failure is desired. Yielding of steel reinforcement followed by FRP rupture or concrete crushing is the optimum scenario for developing the full capacity of externally bonded RC beams.

Anchorage of FRP reinforcement is one of the widely studied solutions to prevent the debonding failure of RC strengthened beams. Many studies have shown that anchoring FRP laminates is effective in delaying or preventing the brittle failure of externally bonded strengthened beams in the form of debonding [10]–[13]. Delaying the debonding failure enhances the fiber utilization and improves the performance of RC beams retrofitted with FRP composites consequently. The main function of the anchorage system is to transfer stresses between the FRP laminate and the concrete substrate which results in arresting the crack propagation [14]. Various anchoring

techniques have been studied in previous research studies, including FRP transverse wrapping, mechanical fasteners, and FRP spike anchors.

FRP transverse wrapping are made of of FRP strips that are oriented perpendicular to the longitudinal axis of the beam [15]–[17]. FRP wraps can be applied continuously over the length of the beam, anchoring the whole length of the FRP laminate. They can also be applied with spacing over the length of the beam or only at the ends. Applying the transverse wrapping at the end primarily prevents concrete cover separation. Wrapping FRP laminates adhered to RC beams can be in the form of complete wraps, U-wraps, or FRP strips. Mechanical anchorage is another way for anchoring FRP sheets where metallic components are used to prevent the debonding of FRP laminates and improve ductility [18]. The main drawback of this type of anchorage is the possibility of corrosion of the mechanical anchors.

FRP anchors consists of a fiber sheet that is bundled and soaked in epoxy resin. Three components form the FRP anchor as shown in Fig. 1 [19]. The dowel is inserted in a predrilled hole in the concrete member, the fan is the portion that is splayed on the FRP sheet with epoxy, the key portion where the fan transitions into the dowel. The insertion angle of the anchor can be 180 degrees resulting in a straight anchor configuration. Anchors can also be inserted inside the concrete with an angle β, forming a bent FRP anchor. Straight anchors utilized for flexural applications are subjected to direct tension. They are mainly applied in structural joints such as beam to slab, slab to wall, and wall to wall continuity as shown in Fig. 2. On the other hand, bent anchors are exposed to both tension and shear forces. They are used for the anchorage of FRP laminates in strengthened beams or slabs.

FRP anchors can be constructed in two ways. A portion of the length of the anchor’s fibers (at least half) can be impregnated or coated with epoxy and allowed to cure before installation. These anchors are called impregnated fiber anchors [20]. The other type of FPR anchors is made of fibers which have not been impregnated in epoxy and placed using the wet lay-up technique. FRP anchors made this way are called dry fiber anchors and they are used in this study.

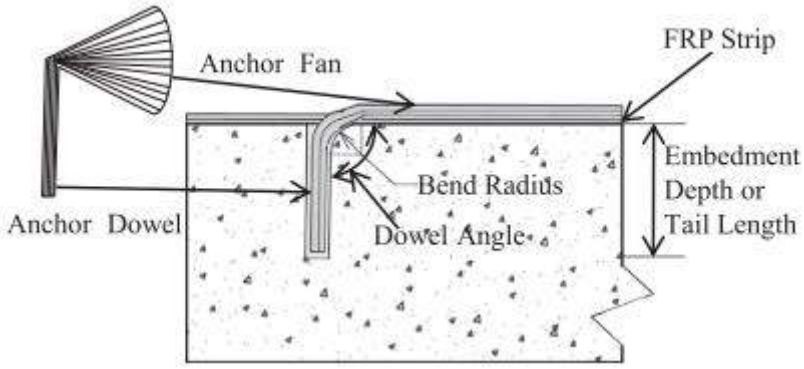

Figure 1: Elements of FRP spike anchors [14]

Figure 2: Applications of straight anchors and bent FRP anchors

There are several parameters that affect the behavior of the FRP-concrete joint system as reported in the literature. These include anchor diameter, fan length, fan angle, embedment length, insertion angle, number of anchors, spacing between the anchors, hole diameter, concrete compressive strength, FRP tensile strength and elastic modulus, and anchor area to sheet ratio (ASR) [20], [21]. Five failure modes of FRP spike anchors were observed in the previous studies. These failure modes are concrete-cone failure, concrete-cone followed by bond failure, dowel pullout, fan-to-sheet debonding and fiber rupture, as shown in Fig. 3. It is vital to avoid all FRP anchor failure modes when designing FRP anchors, to favor rupture in the FRP laminates since the anchors should not limit the strength of the externally bonded (EB-FRP) system [19], [22], [23]

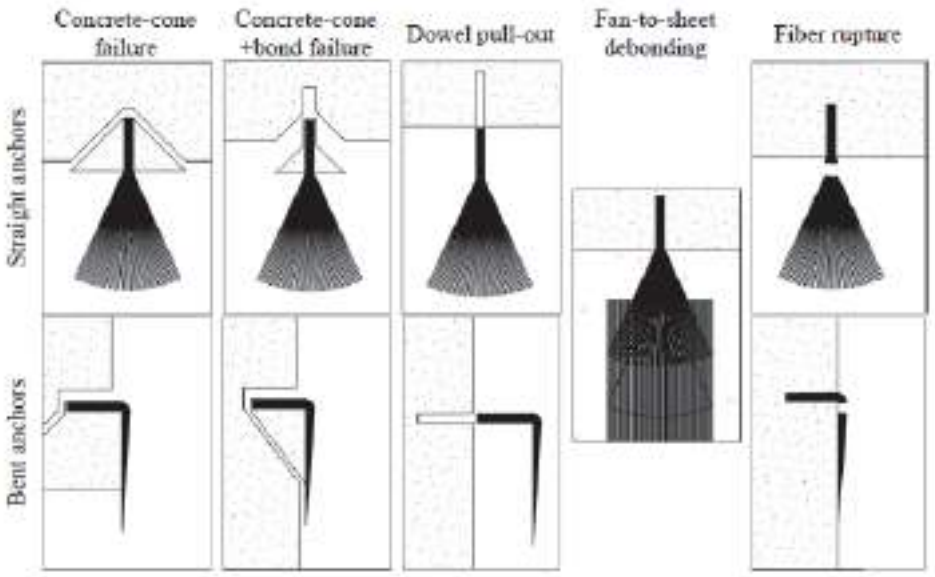

Figure 3: Failure modes of FRP spike anchors [16]

Previous investigation results on FRP anchors design models indicated that the embedment depth of the anchor should be 1.5 times greater than the concrete cover. This is to ensure that the anchor will be able to arrest the crack propagation along the steel reinforcement and thence prevent delamination [19]. Moreover, the embedment depth should be at least 6 times the dowel diameter to prevent concrete cone failure. A linear trend between the anchor capacity and the embedment depth is observed in previous studies [23]–[25]. Nevertheless, Sun et al. [25] stated that increasing the embedment depth beyond a specific value does not increase the bond strength between FRP and concrete. According to Sun [26], it is recommended that the fanning angle should be kept as small as possible (maximum of 32°) since wider fan angles reduce tensile capacity of FRP anchor. In addition, the fan should cover the whole width of the FRP sheet to ensure uniform and consistent stress transfer from the FRP sheet to the concrete substrate [19]. Further, hole diameter should be 3-5 mm larger than anchor dowel diameter to facilitate easier installation [19].

1.2. Research Significance

Structures all around the world are susceptible to deterioration. Although they are designed to have a service life up to 60-80 years, they often need regular maintenance and repairs. The dynamic changes may also increase the loading type or magnitude on the existing structures. Furthermore, some structures are deficient due to

design errors or mistakes during construction. Other structures need upgrading due to temporary overload. To keep these deficient structures in service, they are upgraded, replaced or their use is restricted. These solutions are usually costly and ineffective. Hence, Strengthening is usually needed for various reasons to keep the structures at certain performance level. The most recently used and accepted strengthening materials are the advanced FRP composites which have been widely studied in the last decades. FRP sheets or plates are bonded to the surface of the reinforced concrete (RC) structural member to increase its load carrying capacity. However, the premature debonding of FRP laminates before utilizing the full FRP ultimate strength results in a brittle failure of RC beams.

Several solutions were proposed to solve this problem such as anchoring the FRP laminates. Many anchorage systems were implemented in the field and discussed in the literature. One of the most effective anchoring techniques is the FRP spike anchors. It is proven to mitigate debonding failure and thus enhance the strength and deformability of strengthened beams. However, most of the available data and models on FRP anchors in the literature were obtained from testing small anchors, i.e., anchors with small dimensions, under direct pullout. The models are semi empirical in nature and are limited by the range of experimental data that they were derived from. Therefore, these models could be impractical to apply when designing anchors with larger dimensions and different conditions, especially when implemented in full-scale RC beam specimens. Therefore, it is important to understand the effect of anchors with large dimensions (e.g., diameters larger than 14 mm) on the capacity of the strengthened members. In addition, there is a lack of comprehensive guidelines to design the anchors in the current design codes of practice. As a result, this research aims to investigate the effect of varying different anchor parameters on the capacity of FRP bent anchors. The parameters that will be tested include ASR ratio, anchor diameter, fan length, embedment depth, number, location, and insert angle of anchors. The significance of this study is to optimize the design of FRP spike anchoring systems and to propose design guidelines that could aid engineers and researchers to implement this type of anchors in strengthening applications efficiently.

1.3. Research Objectives

This research aims to study the overall performance of concrete prisms strengthened in flexure with CFRP laminates with different configurations of CFRP splay anchors. The main objectives of this research are:

1. Conduct bending tests on anchored, strengthened, and unstrengthened large-scale reinforced concrete beams to investigate the effect of anchoring FRP-to-concrete joints on the overall behavior of the beams.
2. Compare the load-deflection response curves, flexural capacity, and bond performance of CFRP strengthened, and anchored specimens with that of the control, unstrengthened and unanchored specimens.
3. Study the effect of the anchor fan length, fan angle, dowel angle, and embedment depth on the flexural capacity and ductility of the strengthened and anchored concrete beams.
4. Study the strain in the CFRP laminates and compare the maximum attained strain in the laminates between anchored specimens and unanchored specimens.
5. Compare the experimental results with proposed design guidelines of the anchors in literature.
6. Predict the flexural capacity of the beams using current codes of practice and compare it to the experimentally obtained values of the flexural strength.

Chapter 2. Literature Review

2.1. Flexural Strengthening of Concrete Beams with FRP Laminates

Extensive research has been conducted on the behavior of strengthened concrete beams with different types of FRP laminates. This section summarizes some of the studies and their findings. The majority of the experimental research programs performed on the flexural strength of CFRP-strengthened beams were conducted over a decade ago [9], [27]–[30]. The observed mode of failure of the investigated beams in these studies was mainly debonding of the FRP laminates from the concrete substrate. Consequently, their main conclusions were to recommend the usage of anchorage systems to develop the full FRP strength. Similarly, the dominant mode of failure Obeidat et al. [31] recorded through the testing of 12 RC beams externally bonded with CFRP laminates under four-point bending test was the plate debonding. Leading to an increase of only 7 to 33% in the flexural capacity of the strengthened beams.

Kotynia et al. [6] investigated the parameters that may mitigate the intermediate crack debonding of CFRP laminates through testing 10 rectangular RC beams with varying configurations of FRP wrapping. They tested continuous U-shaped sheets and spaced side-bonded CFRP L-shaped laminates with different fiber orientation. They concluded that the use of transverse FRP continuous U wraps parallel to the beam axis increased the ultimate load carrying capacity. All of the tested specimens in this study failed by intermediate crack debonding of the bottom FRP laminate.

Many studies addressed the reduction in the ductility problem for FRP-strengthened beams through proposing various hybrid strengthening systems [32]–[35]. Attari et al. [35] tested 7 RC beams in flexure, strengthened with different configurations of FRP fabric consisting of glass and carbon. Their findings revealed that using a twin layer of Glass-Carbon fibers increased the capacity of the beams by 114% without a brutal loss in ductility. Chen et al. [36] partially replaced carbon layers with basalt and/or glass fibers to inspect the effect of the hybrid ratio and stacking sequence on the flexural behavior of the laminates. They found that the flexural strength and modulus of the hybrid laminates decreased with the increase in the hybrid ratio of basalt fibers until 50 %. Beyond this ratio, negligible effects on flexural properties were

observed. Moreover, placing basalt or glass in a sandwich-like stacking sequence with a hybrid ratio of 50% achieved a higher flexural strength. The main observation in most of the studies in regard of the effect of the hybridization between CFRP and other FRP laminates with larger rupture strain is the increased ductility of the retrofitted beams.

2.2. Interface Behavior between CFRP and Concrete

Bond performance is a major concern arising when FRP sheets or plates are externally bonded to concrete surfaces. The interface behavior can strictly limit the efficiency of the strengthening system. Numerous research has been carried out to understand the interface mechanisms of the FRP-to-concrete bond.

Bizindavye and Neale [37] defined the transfer length of the bond between a FRP composite and concrete by the distance required for the strain of the bonded joint to reach zero in a pullout shear test. They performed experimental and analytical investigations to study the transfer mechanisms of the FRP-to-concrete bonded joints. They stated that the value of the transfer length is constant for all values of loads before initial cracking. Beyond the cracking load, the transfer length increases with crack propagation. Al-sammari and Breña [38] mentioned that providing anchorage beyond this length has negligible effect in increasing the bond strength between FRP and concrete.

Observations on FRP debonding failure modes in the literature have been classified into four types [7], [39]: (a) concrete cover separation/delamination (b) plate end interfacial debonding (c) intermediate flexural crack induced interfacial debonding (d) intermediate flexural-shear crack induced debonding. As illustrated in Fig. 4, if the high interfacial stresses occur near the end, then delamination or end debonding takes place. On the other hand, debonding can be initiated by flexural or flexural-shear cracks away from the ends which results in intermediate crack induced debonding.

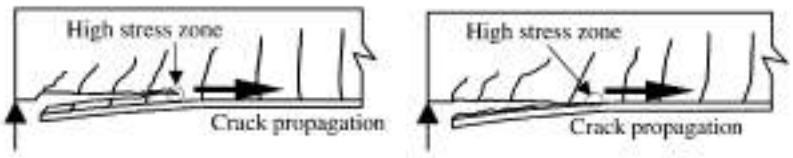

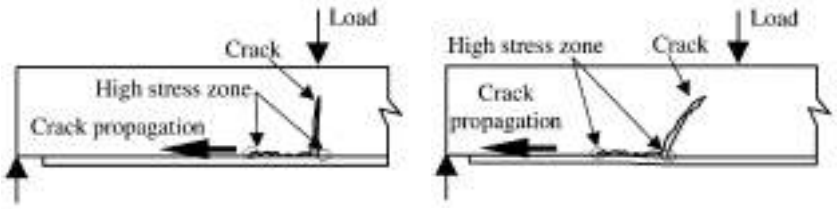

Figure 4: Debonding failure modes mechanism [40]

Yalim et al. [41] examined the effect of concrete surface roughness on the bond behavior of FRP strengthening systems. Their study included the flexural testing of 26 specimens with three different levels of surface roughness. The concrete surface profile did not affect the performance of either the wet layup or precured FRP systems with or without anchorage. They noticed that the type and extent of anchorage affected the mode of failure, specimens with the highest anchorage straps and continuous straps achieved FRP rupture.

2.3. Previous Tests Conducted on CFRP Anchors

Extensive number of tests has been performed on CFRP anchors. Some of the tests were conducted on isolated anchors and others were done on anchors used in combination with externally bonded reinforcement systems. The types of tests presented herein are pullout tests, shear tests, and bending tests.

2.3.1. Pullout tests

Ozbakkaloglu and Saatcioglu [42] tested 81 CFRP anchors under direct pullout test. The test parameters included embedment depth, diameter, angle of inclination, and concrete compressive strength. Anchors were inserted in concrete cylinders of 150 height and either 200- or 270-mm diameter. The tested embedment depths were 25, 50, 75, and 100 mm. The diameter of anchors varied as 12.7, 15.9 and 19.2 mm. Further, 8 of the tested anchors had an angle of inclination measured from the vertical axis that varied from 15 to 45. Pullout of the anchor was the failure mode for most of the specimens whether in the form of concrete pullout or combined cone-bond pullout. Authors concluded that the average bond strength decreased with increasing anchor diameter, embedment depth or inclination angle.

Kim and Smith [20] reported the results of pullout tests on 27 FRP anchors, bonded to concrete prisms of (400×400×150) mm dimensions. The anchor embedment depths varied as 20, 40, and 60 mm. They also varied the anchor hole diameter as 12, 14, and 16 mm. The tested anchor fiber content (which refers to the FRP sheet width that the anchor was made of) were 60, 110, and 130 mm. The failure mode noticed for anchors having a 20 mm depth and different hole diameters was concrete cone failure. The four failure modes of FRP anchors were observed for anchors having a 40 mm embedment depth. Namely, concrete cone failure, combined concrete and bond failure, bond failure, and FRP anchor rupture. However, the 60 mm embedment depth anchors experienced rupture. Authors also compared their results with two previous experimental studies [42], [43] and plotted the pullout load versus the embedment depth as shown in Fig. 5. The trend in Fig. 5 depicts that the pullout load increases with the increase in embedment depth. However, they recommended limiting the embedment depth to avoid high stresses on anchors which could cause anchor rupture. No further conclusions were derived for other tested parameters.

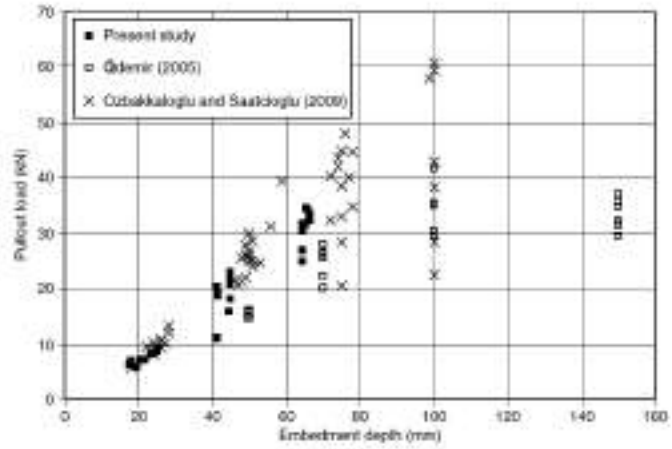

Figure 5: Effect of embedment depth on the pullout capacity of FRP anchors [20]

Authors of the previous paper provided analytical models [44] that quantifies the pullout strength of FRP anchors provided that multiple anchors do not interfere with each other, tension load is applied monotonically, and concrete is uncracked. The analytical model of the pullout strength (N_u) is given as:

$$N_u = \min\left(N_{cc}, N_{cb}, N_{ar}\right) \quad (1)$$

where N_{cc}, N_{cb}, N_{ar} is the pullout strength governed by concrete cone failure, combined con-bond failure, and anchor rupture failure, respectively. They are calculated as follows:

$$N_{cc} = \alpha_{cc} h_{ef}^{1.5} \sqrt{f_c'} \quad (2)$$

$$N_{cb} = \tau_u \pi d_0 h_{ef} \quad (3)$$

$$N_{ar} = \alpha_{ar} w_{FRP} t_{FRP} f_{FRP} \quad (4)$$

where h_{ef} is the effective embedment depth of the anchor (mm), f_c' is the concrete cylinder compressive strength (MPa), d_0 is the diameter of the anchor hole (mm), w_{FRP}, t_{FRP}, and f_{FRP} are the width, thickness, and strength of the fiber sheet used to make the FRP anchor. α_{cc}, τ_u, and α_{ar} are calibration factors determined from a statistical analysis of the different pullout test data test comprising of 84 data points. The resulting calibration factors are 9.68, 4.62, and 9.07, respectively.

It should be noted that the model developed in Eq. (1) is based on existing analytical models for metallic anchors. Authors adopted this strategy due to the abundance in the metallic anchors data, the similarity in the behavior between metallic and FRP anchors, and the limited FRP anchor tests data.

In an experimental investigation carried out by Castillo et al. [22], 32 bent FRP anchors exhibiting rupture failure mode were tested with varied sizes and fanning angle. In the test set-up, the FRP bent anchor is used to connect a RC beam and a RC block as shown in Fig. 6. A previously developed equation for the average value of the ultimate fiber rupture capacity (N_{fr}) was calibrated using the test data for an insertion angle 90°. Also, they performed a statistical study and reported design equations for the 95th percentile and 98th percentile as following:

$$N_{fr}^{95\%} = 2.2 E_{FRP} \varepsilon_{FRP} A_{dowel}^{0.62} \left(\frac{90-\alpha}{90}\right) \quad (5)$$

$$N_{fr}^{98\%} = 1.3 E_{FRP} \varepsilon_{FRP} A_{dowel}^{0.68} \left(\frac{90-\alpha}{90}\right) \quad (6)$$

where α is the fanning angle measured in degrees from the middle to the end of the fanning component.

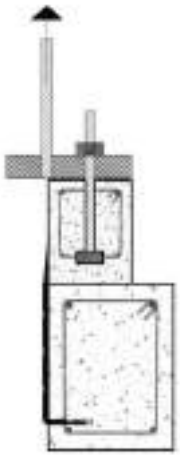

Figure 6: Test setup in Castillo et al. [22]

2.3.2. Single shear tests

Ozbakkaloglu et al. [45] inspected the effect of anchor configuration on the behavior of FRP plates externally bonded to concrete members through single shear pull-off tests. They tested 33 specimens of 350 mm length, 150 mm height, and 25 mm width. The anchors configuration varied as single, double, or multiple anchors in the longitudinal or transverse direction. Their results indicated that peak loads and ductility increase with the increase in anchors numbers and embedment depths. Moreover, the peak load decreased with the increase in the distance between anchors and loaded ends.

Flores et al. [46] proposed an empirical model that is based on their experimental work and previous existing single shear tests in the literature to estimate the CFRP anchored joint's strength. They assumed that the joint capacity is the added contribution of the anchor and the bond strength. The model accounted for the influence of the FRP sheet width, the bonded length behind the anchor, and the anchor fan position with respect to the FRP longitudinal sheets (expanded onto the sheet or between two plies). The anchored joint strength can be calculated as follows:

$$P_{ancjoint} = P_{db} + nk_{glob}.P_{anc} \quad (7)$$

where P_{db} is the FRP-to-concrete bond strength, n is the number of anchors distributed transversally in one row, P_{anc} is the anchor's strength, and k_{glob} is a

factor that accounts for the three mentioned parameters, it is evaluated by a simple expression obtained using least square regression.

Al-Sammari and Breña [47] proposed an anchorage efficiency factor that accounts for the effect of using CFRP spike anchors with externally bonded CFRP sheets on RC beams. They performed finite element (FE) analysis using ABAQUS as shown in Fig. 7, and conducted a parametric study to derive an equation that predicts the increase in strain utilization by accounting for several factors. Namely, number of anchor rows, CFRP sheet fiber thickness, spacing between the anchors, anchor embedment depth, and anchor fan diameter. They compared the calculated results with values obtained from previous experimental tests and the difference between the results did not exceed 15%. They also verified their FE model using test results from previous experimental investigations. The simplified form of the equation they proposed for the anchorage efficiency factor which shall be multiplied by the original ACI-440.2R-17 [48] equation for debonding strain is:

$$K_{\varepsilon a} = 1 + \alpha_c \sqrt{\frac{t_f a_d}{3 S_a}} n_a^2 \tag{9}$$

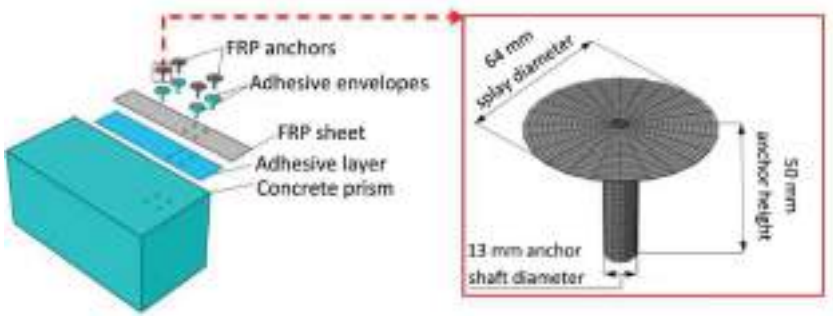

Figure 7: Finite element model components in [47]

where α_c is a calibrated factor that accounts for the difference in behavior when the spacing between anchors approaches the length of the effective stress transfer zone. When n_a= 1, α_c=3/8 and S_a=1/3 where n_a is the number of anchor rows and S_a is the center to center spacing between anchors. t_f is the CFRP sheet thickness and a_d is the anchor shaft diameter.

2.3.3. Bending tests

Zaki et al. [49] tested three full scale T-beams and another three rectangular beams under four-point bending test. The beams contain one control specimen of each type, and the rest are strengthened with CFRP sheets and anchored along the shear span using either U-wraps or FRP anchors. The diameters of the used FRP anchors were 16 and 19 mm, with 203 and 140 mm spacing, respectively. On half of the span of the anchored beams, dowel (impregnated) anchors were used while bundled fibers were used on the other half. They observed that the use of smaller and closely spaced FRP anchors is more effective than using larger and more widely spaced anchors. They also reported that the dowel anchors offer higher stiffness and strength than the fiber anchors, but the fiber anchors offer slightly more deformability in shear. Finally, they proposed a multiplier coefficient for the ACI440.2R-17 [48] equation of debonding strain. This multiplier account for the development in strain as a result of the sheets anchorage and was found by dividing the load at experimental failure by the predicted load at FRP debonding strain. The highest multiplier value corresponded to the T-beam having 16 mm diameter anchors and it was 1.66. The rectangular beam anchored with 19 mm anchors had the lowest multiplier value of 1.11.

Sun et al. [50] suggested a new anchoring technique consisting of FRP spike anchors between two patches of FRP sheets as shown in Fig. 8. They conducted 21 experiments to study the performance of such anchorage system. They tested concrete blocks of (152×152×610) mm dimensions under three-point bending test. Compared with conventional spike anchors, the proposed anchorage system showed an improved behavior in terms of utilization of EB FRP sheets, even with s sharp corner (i.e., bent radius equals zero). They also noticed that reducing the fanning angle prevents the unfavorable failure of anchor-sheet delamination and anchor rupture. (u-shape to prevent concrete shear failure). In another study published by Sun et al. [23], they used the experimental results from 64 tests on anchors that failed in rupture to evaluate the anchor strength using the existing equations in the literature. A comprehensive equation was proposed to account for the impacts of embedment depth, bend ratio, strength ratio, and dowel angle on the anchor strength:

$$f_{fb} = [(0.06r_b + 0.21) + 0.22S_{ratio}^{-1.15} + 0.23(\frac{\alpha_d}{90^\circ} - 1)]f_{fu} \quad (10)$$

where f_{fb} is the anchor strength, r_b is the bend ratio (the ratio of the bend radius to the diameter of the spike anchor), S_{ratio} is the strength ratio of FRP strength to FRP reinforcement, α_d is the dowel angle, and f_{fu} is the strength of the FRP reinforcement.

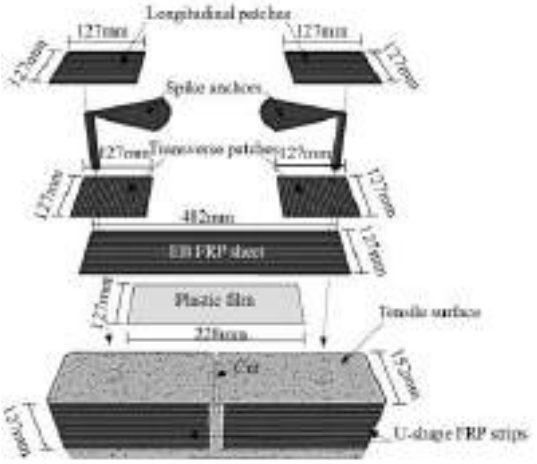

Figure 8: Proposed method of anchorage [50]

Castillo et al. [14] provided a concise review on the behavior of FRP anchors in combination with EBR systems. They compiled the results from previous research programs that tested isolated FRP anchors and others that tested FRP anchors when used with EBR systems in strengthening RC structures. They also reported previously published design models related to different failure modes. Namely, Kim and Smith [44] model for calculating strength of straight anchors exhibiting pull-out and concrete cone failure, Villanueva Llaurado [24] equation which predicts the tensile capacity of bent anchors that fail by rupture. Authors also reported the shortcomings related to these models. For instance, the former model used limited range of parameters and there was no further corroboration of the model by other investigators. All anchors tested by the latter model had the same size and a fanning angle of zero. This means that the anchor end outside of the concrete was bundled which contradicts the typical configuration of bent anchors that are usually fanned out. The two models are presented herein:

Kim and Smith [44]: $N_{cc} = 9.68 d_e^{1.5} \sqrt{f_c'}$ (11)

$$N_{cb} = 4.62 \pi \emptyset_{dowel} d_e \text{ when } f_c' < 20\ MPa \quad (12)$$

$$N_{cb} = 9.07 \pi \emptyset_{dowel} d_e \text{ when } f_c' \geq 20\ MPa \quad (13)$$

where N_{cc} and N_{cb} is the capacity of the anchor exhibiting concrete cone failure and combined concrete and bond failure, respectively. d_e is the hole diameter in mm and $\emptyset_{dowel}$ is the dowel diameter in mm.

Villanueva Llaurado [24]: $V_{fr} = 0.002 A_{dowel} f_{FRP} (h_{ef} + 50 r_b \frac{\beta}{\pi})$ (14)

where V_{fr} is the average tensile capacity of bent anchors, A_{dowel} is the cross-sectional area of the anchor in mm^2, and f_{FRP} is the ultimate tensile strength of the sheet used to manufacture the anchor in MPa. h_{ef} is the embedment depth in mm, r_b and β are the bend ratio at the key portion and the insertion angle in degrees, respectively.

Shekarchi et al. [51] provided recommendations on the design of CFRP splay anchors. The proposed design guidelines were developed based on 51 small-scale tests. Three-point bending test was performed on beam specimens having two groups of dimensions: the first group is from sun [52] and were 152 mm wide, 152 mm tall, and 610 mm long. The second group of beam specimens is taken from Pudleiner [53] and had dimensions of 305 mm width, 305 mm depth, and 1727 mm length. From the analysis of the database results, authors recommended the following design guidelines in order to develop the full capacity of the FRP strips. Firstly, the anchor to the FRP strip's area (ASR) ratio should not be less than 2.0. Secondly, the anchor hole should be at least 1.4 times larger than the equivalent laminate area of the CFRP anchors. Also, the anchor chamfer radius should be 1.4 times the anchor hole radius.

2.4. Flexural Capacity Predictions of FRP-Strengthened RC Beams

This section provides the design guidelines of RC beams strengthened with FRP in flexure. The mentioned guidelines are in accordance with ACI 440.2R-17 [48], CSA-S806.12 (R 2017) [59], (fib) bulletin 90 (2019) [60].

2.4.1. American concrete institute design guidelines for flexural strength (ACI 440.2R-17) [53]

This section presents the detailed equations provided by ACI 440.2R-17 [48] for the design of externally bonded reinforcement to RC beams.

The nominal flexural strength of the concrete structure should exceed the factored moment as indicated by Eq. 15.

$$\emptyset M_n \geq M_u \tag{15}$$

where:

M_u= factored ultimate moment calculated by the ACI 318-19 code .

$\emptyset$= strength reduction factor calculated by the following equation:

$$\emptyset = \begin{cases} 0.90 \; for \; \varepsilon_t \geq 0.005 \\ 0.65 + \frac{0.25(\varepsilon_t - \varepsilon_{sy})}{0.005 - \varepsilon_{sy}} \; for \; \varepsilon_{sy} < \varepsilon_t < 0.005 \\ 0.65 \; for \; \varepsilon_t \leq \varepsilon_{sy} \end{cases} \tag{16}$$

M_n = nominal strength of the member calculated by the following equation:

where:

ε_t = net tensile strain in extreme tension steel at nominal strength (mm/mm)

ε_{sy}= steel yield strain (mm/mm)

$$M_n = A_s f_y \left(d - \frac{\beta_1 c}{2}\right) + \Psi_f A_f f_{fe} \left(d_f - \frac{\beta_1 c}{2}\right) \tag{17}$$

where:

ψ_f = FRP strength reduction factor, taken as 0.85.

A_s = area of steel reinforcement (mm^2)

f_s = stress in tensile steel reinforcement (MPa), calculated by Eq. 10

d = effective depth of tensile steel reinforcement (mm)

β_1 = concrete stress block factor dependent on failure mode

c = depth of neutral axis (mm) (initially assumed) calculated by Eq. 12

A_f = area of FRP reinforcement = $nt_f w_f$

n = number of FRP layers

t_f = thickness of FRP sheet (mm)

w_f = width of FRP sheet (mm)

f_{fe} = effective stress in FRP reinforcement (MPa), calculated by Eq. 8

d_f = effective depth of the FRP reinforcement (mm)

The flexural capacity of the RC sections strengthened with externally bonded FRP is controlled by the governing failure mode. If the strain in the concrete (ε_c) reaches the maximum usable strain in compression (ε_{cu}), concrete crushing is assumed to occur. If the strain in the FRP (f_{fe}) reaches its design rupture strain (ε_{cu}) before the concrete reaches the crushing strain, FRP is assumed to rupture. However, FRP debonding and concrete cover delamination occurs when bond failure takes place due to high interfacial shear stresses. This type of failure is considered brittle, and to prevent such failure, the effective strain of FRP reinforcement (ε_{fe}) calculated by Eq. 18 is limited by the debonding strain (ε_{fd}) as defined in Eq. 19.

$$\varepsilon_{fe} = \varepsilon_{cu}\left(\frac{d_f - c}{c}\right) - \varepsilon_{bi} \leq \varepsilon_{fd} \tag{18}$$

$$\varepsilon_{fd} = 0.41\sqrt{\frac{f_c'}{nE_f t_f}} \leq 0.9\varepsilon_{fu} \tag{19}$$

where:

f_c' = compressive strength of concrete (MPa)

E_f = elastic modulus of FRP laminates (MPa)

ε_{fu} = FRP rupture strain (mm/mm)

ε_{bi} = initial strain in the substrate (mm/mm)

The effective strain in the flexural FRP can reach the ultimate rupture value if FRP sheets are properly anchored so that the debonding failure is delayed or prevented. In this case, the strain in the FRP is assumed to reach the rupture strain. The effective stress in the FRP (ε_{fe}) is the maximum level of stress developed by the FRP reinforcement before flexural failure and could be obtained by Eq. 20 from the strain in the FRP assuming a perfectly elastic behavior.

$$\varepsilon_{fe} = \varepsilon_{cu}\left(\frac{d_f - c}{c}\right) - \varepsilon_{bi} \leq \varepsilon_{fd} \tag{20}$$

The strain in the steel reinforcement (ε_s) is found by Eq. 21 using strain compatibility. The stress in steel (f_s) is then computed assuming elastic-perfectly plastic steel stress-strain curve using Eq. 22.

$$\varepsilon_s = (\varepsilon_{fe} + \varepsilon_{bi})\left(\frac{d-c}{d_f-c}\right) \tag{21}$$

$$f_s = E_s\varepsilon_s \leq f_y \tag{22}$$

where:

where:

E_s = steel elastic modulus (MPa)

f_y = steel yield stress (MPa)

The strain in concrete is calculated by similar triangles using the following equation:

$$\varepsilon_c = (\varepsilon_{fe} + \varepsilon_{bi})(\frac{c}{d_f-c}) \tag{23}$$

With the strain and stress level in FRP and steel determined for an assumed neutral axis (c), the internal force equilibrium should be checked by the following equation:

$$c = \frac{A_s f_s + A_f f_{fe}}{\alpha_1 f_c' \beta_1 b} \tag{24}$$

If concrete crushing controls and $\varepsilon_{fe} \leq \varepsilon_{fd}$ then: $\alpha_1 = 0.85$ and β_1 is calculated by the following formula:

$$\beta_1 = \begin{cases} 0.85 \; for \; f_c' \leq 28 \; MPa \\ 0.85 - 0.00714(f_c' - 28) \; for \; 28 < f_c' < 56 \; MPa \\ 0.65 \; for \; f_c' \geq 56 \; MPa \end{cases} \tag{25}$$

If concrete crushing did not govern, $\alpha_1$and β_1 should be calculated by the following equations:

$$\beta_1 = \frac{4\varepsilon'_c - \varepsilon_c}{6\varepsilon'_c - 2\varepsilon_c} \tag{26}$$

$$\alpha_1 = \frac{3\varepsilon'_c\varepsilon_c - \varepsilon_c^2}{3\beta_1\varepsilon'^2_c} \tag{27}$$

$$\varepsilon'_c = \frac{1.7\, f'_c}{E_c} \tag{28}$$

The service stresses in the reinforcing steel ($f_{s,s}$), FRP ($f_{f,s}$) and concrete ($f_{c,s}$), are checked using equations (29) – (31).

where:

ε'_c = strain in concrete at compressive strength (mm/mm)

E_c = concrete elastic modulus (MPa) calculated as $4700\sqrt{f'_c}$

$$f_{s,s} \leq 0.80 f_y \tag{29}$$

$$f_{c,s} \leq 0.60 f'_c \tag{30}$$

$$f_{f,s} \leq \begin{cases} 0.2\, f_{fu} \text{ for GFRP} \\ 0.3\, f_{fu} \text{ for AFRP} \\ 0.55\, f_{fu} \text{ for CFRP} \end{cases} \tag{31}$$

where:

$f_{s,s}$ = stress in flexural steel reinforcement (MPa), calculated by the following equation:

$$f_{s,s} = \frac{\left[M_s + \varepsilon_{bi} A_f E_f \left(d_f - \frac{kd}{3}\right)\right](d-kd)E_s}{A_s E_s \left(d - \frac{kd}{3}\right)(d-kd) + A_f\, E_f \left(d_f - \frac{kd}{3}\right)(d_f - kd)} \tag{32}$$

$f_{c,s}$ = stress in concrete (MPa), calculated by the following equation:

$$f_{c,s} = \frac{M_s}{I_{cr}} n \tag{33}$$

$f_{f,s}$ = stress in FRP reinforcement (MPa)

$$f_{f,s} = f_{s,s,} \left(\frac{E_f}{E_s}\right) \left(\frac{d_f - kd}{d - kd}\right) - \varepsilon_{bi} E_f \tag{34}$$

f_{fu} = FRP rupture stress (MPa)

M_s = moment at service load (N-mm)

kd = depth of the neutral axis at service (mm).

I_{cr} = moment of inertia of cracked section (mm^4)

$n =$ concrete modular ratio which calculated by $\frac{E_s}{E_c}$

2.4.2. Canadian standards association CSA-S806.12 (R 2017) [59]

The nominal flexural moment of a strengthened section is calculated as explained previously:

$$M_n = A_s f_y \left(d - \frac{\beta_1 c}{2}\right) + A_F f_F \left(d_f - \frac{\beta_1 c}{2}\right) \quad (35)$$

The debonding strain in the FRP is denoted by ε_{Fmax} and is calculated by equation (36):

$$\varepsilon_{Fmax} = 0.41\sqrt{\frac{f_c'}{n_f E_f t_f}} \leq 0.007 \quad (36)$$

The procedure is similar to the previous explained guidelines by the ACI-440, the only difference is in the calculation of α_1 and β_1:

$$\text{If } \left(\frac{c}{d}\right) \geq \frac{7}{7+2000\varepsilon_{Fu}}: \quad (37)$$

$$\alpha_1 = 0.85 - 0.0015 f_c' \geq 0.67$$

$$\beta_1 = 0.97 - 0.0025 f_c' \geq 0.67$$

2.4.3. International federation for structural concrete (fib) bulletin 90 (2019) [60]

The nominal flexural moment of the strengthened section (M_n) can be calculated from equation (38):

$$M_n = A_{s1}\,\sigma_{s1}\,(d_{s1} - k_2 x) + A_f\,E_f\,\varepsilon_f\,(h - k_2 x) + A_{s2}\,\sigma_{s2}\,(k_2 x - d_{s2}) \quad (38)$$

where:

A_{s1}: area of bottom steel reinforcement (mm^2)

A_{s2}: area of top steel reinforcement (mm^2)

σ_{s1}: stress in the bottom steel reinforcement (MPa) and can be calculated using equation (39):

$$\sigma_{s1} = \min\left(\varepsilon_c \frac{d_{s1}-x}{x}, \frac{f_{yd}}{E_s}\right) E_s \quad (39)$$

σ_{s2} : stress in the top steel reinforcement (MPa), calculated by:

$$\sigma_{s2} = \min\left(\varepsilon_c \frac{x-d_{s2}}{x}, \frac{f_{yd}}{E_s}\right) E_s \quad (40)$$

d_{s1}: distance from extreme compression fiber to centroid of tension reinforcement (mm)

d_{s2}: distance from extreme compression fiber to centroid of compression reinforcement (mm)

h: overall height of the member (mm)

x: depth of the neutral axis (mm)

k_1 and k_2: factors for the average compressive stress and the lever arm of the parabolic-rectangular stress distribution of concrete calculated using the following equations:

$$k_1 = \begin{cases} 1000\varepsilon_c\left(0.5 - \frac{1000}{12}\varepsilon_c\right) \; for \; \varepsilon_c \leq 0.002 \\ 1 - \frac{2}{3000}\varepsilon_c \; for \; 0.002 \leq \varepsilon_c \leq 0.0035 \end{cases} \quad (41)$$

$$k_2 = \begin{cases} \frac{8-1000\varepsilon_c}{4(6-1000\varepsilon_c)} \; for \; \varepsilon_c \leq 0.002 \\ \frac{1000\varepsilon_c(3000\varepsilon_c-4)+2}{2000\varepsilon_c(3000\varepsilon_c-2)} \; for \; 0.002 \leq \varepsilon_c \leq 0.0035 \end{cases} \quad (42)$$

Strain in the FRP reinforcement is calculated by strain compatability and should not exceed the design strain ($\varepsilon_{fbd,IC}$):

$$\varepsilon_f = \varepsilon_c \frac{h-x}{x} \leq \varepsilon_{fbd,IC} \quad (43)$$

Using the simplified stress method:

$$\varepsilon_{fbd,IC} = \frac{f_{bd.IC}}{E_f} \quad (44)$$

where $f_{bd.IC}$ is the design stress in the FRP reinforcement, calculated by the following equation:

$$f_{bd.IC} = \frac{k_{cr,k}\, k_k k_b \sqrt{\frac{2E_f}{t_f} f_{cm}^{\frac{2}{3}}}}{\gamma_{fb}} \quad (45)$$

k_{cr} and k_k are numerical coefficients, taken as 1.8 and 0.17, respectively.

γ_{fb} is a partial factor, taken as 1.5.

k_b is the shape factor, calculated as per the following equation:

$$k_b = \sqrt{\frac{2-\frac{b_f}{b}}{1+\frac{b_f}{b}}} \geq 1 \quad (48)$$

where b_f is width of FRP reinforcement (mm) and b is width of the member (mm).

fib 14 also predicts the strain at which the delamination may occur ($\varepsilon_{f,CD}$), the equation used to calculate the delamination strain is:

$$\varepsilon_{f,CD} = \frac{N_{f,max}}{A_f E_f} \quad (49)$$

where $N_{f,max}$ is the maximum force in the FRP laminate, calculated by equation 50:

$$N_{f,max} = \alpha C_1 k_c k_b b \sqrt{E_f t_f f_{ctm}} \quad (50)$$

where:

α is a reduction factor to account for the effect of inclined cracks and is equal to 0.9. k_c is a factor that accounts for compacted surface and is taken as 1.0, k_b is a geometry factor taken as 1.03, C_1 is taken as 1. b is the width of the beam and f_{ctm} is the modulus of rupture for concrete.

If the FRP laminates are properly anchored, *fib* 14 permits to assume that the resisting FRP force may reach the tensile strength of the material. However, the stress should be limited to $0.9f_{fd}$.

Chapter 3. Experimental Program

3.1. Specimen Details

A total of 17 reinforced concrete beams were cast and tested. The beams had a span of 2 m and a width of 200 mm. The total height of the beams was 250 mm with an effective depth of 204 mm as shown in Fig. 9. They were reinforced with 2Ø12 rebars in tension and 2Ø8 bars in compression. The shear reinforcement consists of Ø10 stirrups at 100 mm spacing. The flexural strengthening of the beams consists of one ply of CFRP bonded to the tension side (bottom of the beams). The CFRP sheets are 150 mm in width and 1600 mm in length and are bonded to the concrete at a distance 200 mm away from each end. In addition, CFRP anchors were installed in predrilled holes at 300 mm away from each end of the beam. The strengthened RC beam section details are shown in Figs. 10-11. Two specimens out of the seventeen acted as benchmark specimens. One specimen was left without strengthening, and the other one was strengthened with one layer of unanchored CFRP laminates. The rest of the specimens were externally reinforced with different configurations of anchors.

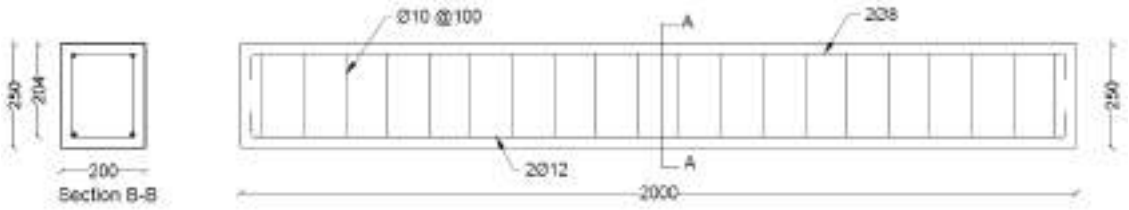

Figure 9: Schematic of the RC beam (dimensions in mm)

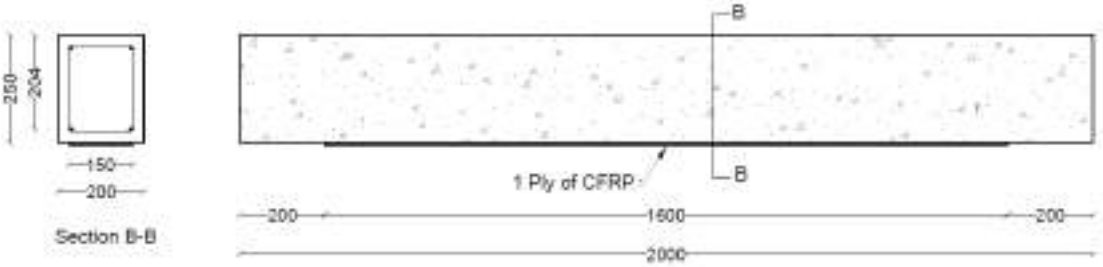

(a)

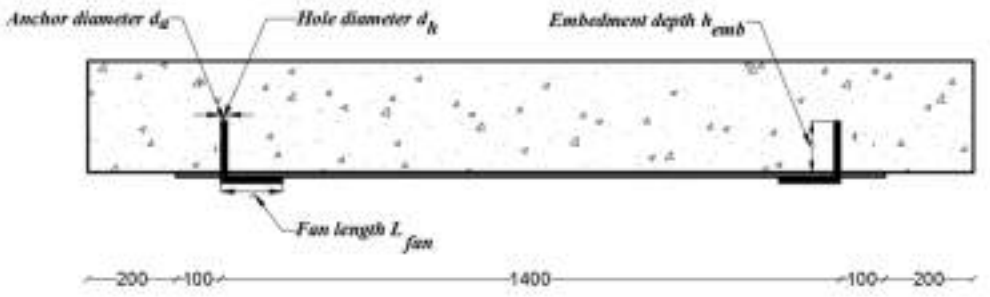

(b)

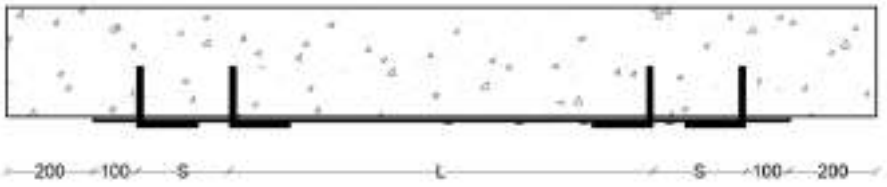

(c)

(d)

Figure 10: Strengthening and anchor detailing of the beams with: (a) FRP laminate; (b) FRP laminate with two anchors; (c) FRP laminate with four anchors; (d) FRP laminate with inclined anchors

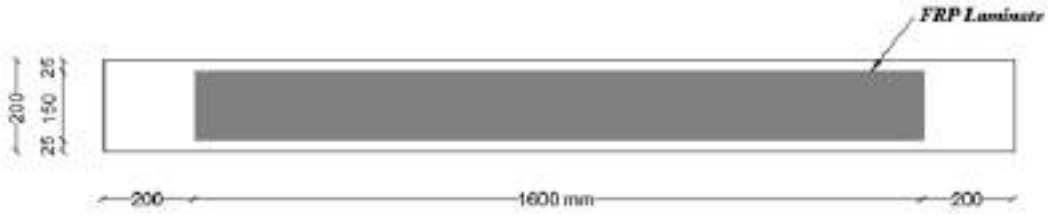

(a)

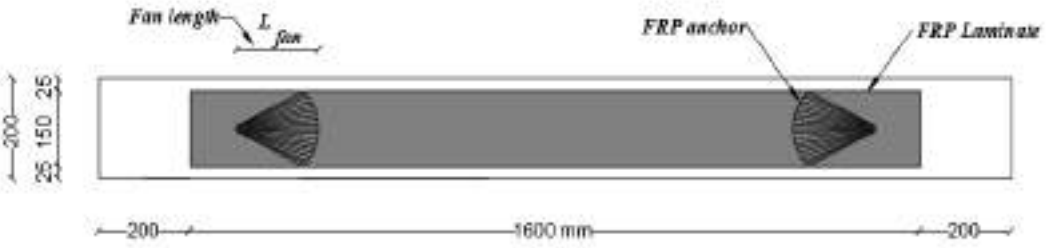

(b)

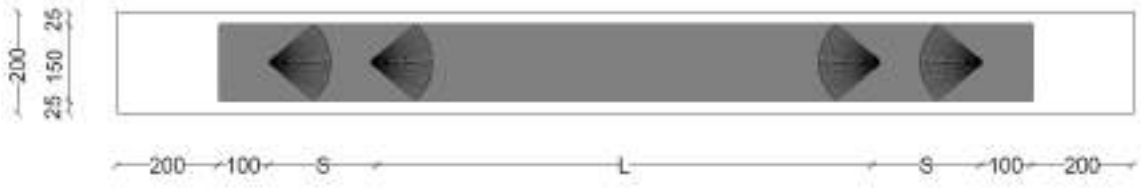

(c)

Figure 11: Bottom view of strengthened beam specimens with: (a) FRP laminate; (b) FRP laminate and two anchors; (c) FRP laminate and four anchors

3.2. Material Properties

3.2.1. Concrete.

The beams were cast using normal weight concrete. Concrete cubes and cylinders were cast and tested after 7 days, 28 days and on the testing day. Compressive strength tests were performed in American University of Sharjah's Asphalt lab in accordance with ASTM C109/C109M-16a [54] standards at stress control rate of 0.25 MPa/sec. Table 1 shows the compressive strength results. Moreover, Fig. 12 shows a cube sample in the crushing machine and Fig. 13-a, 13-b show a cylinder and a cube sample after failure.

Table 1: Concrete compressive strength results.

	Sp. No.	**7 days**		**28 days**		**Testing day**	
		f_{cu}	f'_c	f_{cu}	f'_c	f_{cu}	f'_c
Cubes	1	35.15	29.17	53.44	44.35	54.09	44.89
	2	31.24	25.93	48.73	40.45	55.83	46.33
	3	30.73	25.51	53.22	44.17	58.90	48.88
Average		32.37	26.87	51.80	42.99	56.27	46.70
Cylinders	**Sp. No.**	f'_c		f'_c		f'_c	
	1	28.81		44.15		45.33	
	2	27.97		42.53		42.93	
	3	29.00		45.37		46.45	
Average		28.59		44.02		44.90	

Figure 12: Compressive strength testing machine

(a) Typical failure of a concrete cylinder

(b) Typical failure of a concrete cube

Figure 13: Failure of concrete samples

3.2.2. Steel reinforcement. Steel bars of diameters 12 mm and 8 mm were used to reinforce the beams in flexure in the tension and compression zones, respectively. In addition, stirrups of diameter 8 mm were used as shear reinforcement. Tensile strength tests on coupon specimens were conducted to find the mechanical properties of steel reinforcement according to ASTM A370-18 [54] standards as shown in Fig. 14. Three

coupon tests were conducted on steel bars of diameter 12 mm. The results of the tensile tests are reported in Table 2.

Table 2: Mechanical properties of steel bars

Bar Diameter (mm)	f_y **(MPa)**	E **(GPa)**	f_u **(MPa)**	ε_{rup} **(%)**
12-1	569	199.9	654	8.20
12-2	574	199.9	660	7.80
12-3	561	197.2	646	8.00
Average	568	199	653.3	8.00

(a) Steel test instrumentation

(b) Typical failure of steel bars

Figure 14: Tensile strength test of steel bars

3.2.3. CFRP sheets and epoxy. The CFRP sheets consists of high strength unidirectional CFRP material. The dry and laminate (fiber + epoxy) properties of CFRP sheets as provided by the manufacturer are presented in Table 3. In addition, the mechanical properties of the primer and epoxy resin used for impregnation of the laminates and anchors are presented.

Table 3: Properties of dry CFRP sheets and anchors, CFRP laminates (sheets with epoxy), and epoxy adhesive

Material		Thickness (mm)	Elastic Modulus (GPa)	Tensile strength (MPa)	Elongation at failure (%)
CFRP sheets and anchors	V-Wrap™ C200HM-N	-	289.550	5440	1.90
CFRP laminates	V-Wrap™ C200HM-N	1.02	73.770	1240	1.1
Epoxy Adhesive	V-Wrap™770	-	2.760	60.7	4.4

3.3. Test Matrix

This study investigates the effect of different FRP anchor parameters including anchor diameter, anchor inclination angle (dowel angle), embedment depth, fan length and number of anchors on the flexural capacity of full-scale RC beams. The test matrix of this study is summarized in Table 4. As shown in the table, four anchor diameters (14, 20, 22, and 24 mm) were investigated. The choice of large diameters was selected since the literature lacks information on the behavior of anchors with diameters greater than or equal to 20 mm. The embedment depth was designed according to the common practices in the field as a value greater than or equal to six times the anchor diameter ($6d_a$). Also, lesser values of embedment depth than the limit were investigated to check if the limit is critical for the development of adequate flexural strength.

The ASR values varied from 1 to 3 as shown in Table 4. These values were calculated as per Eq. (51). Several studies recommended a value of ASR to be greater or equal to 2 to limit the probability of anchor rupture failure [26]. However, in this study the feasibility of anchors with an ASR of 1 was investigated, therefore reducing the amount of FRP used to make the anchors.

$$ASR = \frac{A_a}{A_s} = \frac{N_a \frac{\pi}{4} d_a^2}{n w_s t_s} \quad (51)$$

where, A_a is the cross-sectional are of the FRP anchor (mm^2); A_s cross-sectional area of the FRP laminate (mm^2); $N_a$is the number of anchors; d_a is the diameter of the

anchor dowel (mm); n is the number of FRP plies; w_s is the width of the FRP strip (mm); and t_s is the thickness of the FRP strip (mm).

The fan length (l_{fan}) is a function of the interlaminate bond strength and anchor stiffness. Due to unavailability of design models that incorporate the fan length, the ACI440.2R-17 [48] equation of the minimum development length of FRP (l_{ds}) was conservatively used to calculate the anchor fan lengths. It should be noted that Eq. (52) accounts for FRP-to-concrete bond strength and not the interlaminate bond strength and is therefore considered conservative. Rearranging Eq. (52) to include the CFRP anchor properties, Eq. (53) was derived, which was used to calculate the fan lengths (l_{fan}) of the specimens. In this study, the values of the fan lengths varied between the specimens to incorporate a range of numbers less, more, and equal to the calculated l_{fan} values as given in Table 1.

$$l_{ds} \geq \sqrt{\frac{nE_f t_f}{\sqrt{f'_c}}} \tag{52}$$

$$l_{fan} \geq \sqrt{\frac{E_{anc}A_{anc}}{w_{anc}\sqrt{f'_c}}} \tag{53}$$

where, n is the number of FRP plies; E_f is the elastic modulus of FRP (MPa); t_f is the thickness of the FRP laminate (mm); f'_c is the compressive strength of concrete (MPa); E_{anc} is the elastic modulus of the FRP anchor (MPa); A_{anc} is the anchor cross-sectional area (mm^2); and w_{anc} is the width of the anchor sheet (mm).

The designation of the specimens anchored with two anchors starts with A, followed by the diameter of the anchors. The embedment depth and fan length values are reported in the specimens' designation in (mm) following the letter H or F, respectively. for example, specimen A14-H80-F180 refers to a strengthened and anchored beam with two 14 mm anchors, having embedment depth of 80 mm, and fan length of 180 mm. Number 4 is inserted at the beginning of the two specimens' names that are anchored with 4 anchors. The designations of the specimens having inclined anchors start with IA. Unstrengthened and unanchored specimens are pointed out as C and UA, respectively.

Table 4: Test matrix

Designation	Anchor Detailing				
	Embedment Depth (mm)	Insertion Angle (°)	Diameter (mm)	Fan Length (mm)	ASR
Group 1 (Control Beams)					
B	-	-	-	-	-
BU	-	-	-	-	-
Group 2 (14 mm diameter, 2 anchors)					
A14-H80-F180	80	90	14	180	1.0
A14-H80-F120	80	90	14	120	1.0
A14-H100-F180	100	90	14	180	1.0
Group 3 (14 mm diameter, 4 anchors)					
4A14-H100-F180	120	90	14	180	2.0
4A14-H80-F120	80	90	14	120	2.0
Group 4 (20 mm diameter)					
A20-H120-F260	120	90	20	260	2.1
A20-H100-F260	100	90	20	260	2.1
Group 5 (22 mm diameter)					
A22-H140-F280	140	90	22	280	2.5
A22-H160-F280	160	90	22	280	2.5
A22-H140-F220	140	90	22	220	2.5
Group 6 (24 mm diameter)					
A24-H150-F300	150	90	24	300	3.0
A24-H120-F300	120	90	24	300	3.0
A24-H150-F260	150	90	24	260	3.0
Group 7 (Inclined anchor)					
IA14-H100-F180	100	45	14	180	1
IA20-H100-F260	100	45	20	260	2.1

3.4. Test Setup

All beams were tested under four-point bending tests in a Universal Testing Machine (UTM) under a displacement-controlled rate of 2 mm/min. To measure the deflection of the specimens, one linear variable differential transformer (LVDT) was placed under the beam's soffit as shown in Fig. 15 and Fig. 16. One strain gauge was mounted onto the concrete near the top mid-span of the beams to monitor the strain in the concrete. In addition, two strain gauges were fixed on the bottom steel bars to

measure the strain in the flexural steel reinforcement. Furthermore, a strain gauge was placed on the CFRP laminates at midspan to measure and study the CFRP strain distribution in the unanchored and anchored laminates.

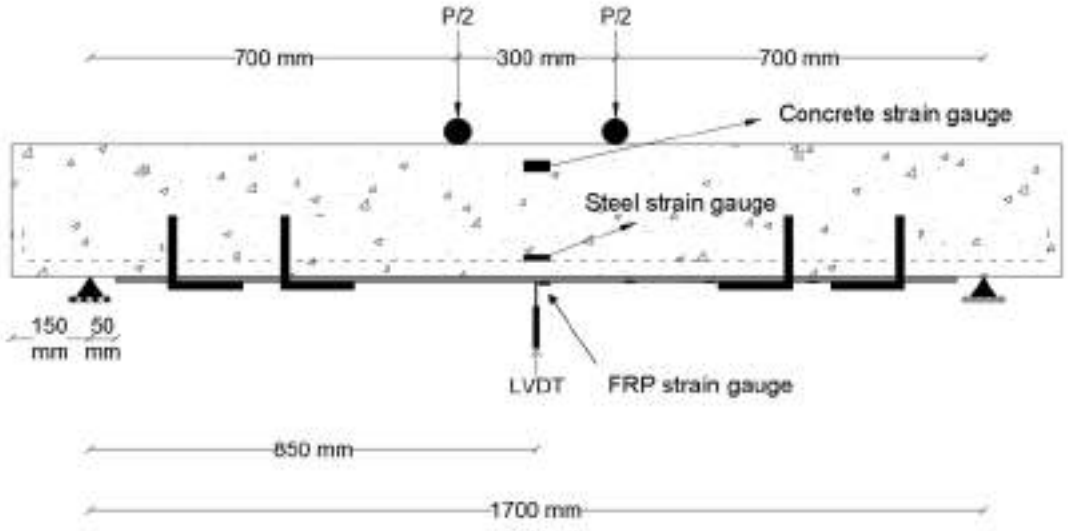

Figure 15: Schematic of the test setup

Figure 16: Test setup

3.5. Preparation and Strengthening of Specimens

3.5.1. Preparation of RC beams

First, steel reinforcement and formwork were prepared as shown in Fig. 17-a. Grinding of the bottom steel bars at the location of the strain gauges was done and strain gauges were fixed in these locations. After that, the steel cage was inserted in the formwork and concrete was casted. Vibration was performed to ensure that no air bubbles are entrapped in the concrete. When the formwork was filled with concrete, the concrete surface was levelled as illustrated in Fig. 17-b. The beams were left to cure for 7 days before starting the strengthening process.

(a) Steel cage and formwork (b) Leveling concrete surface (c) Casted concrete beams

Figure 17: Casting of specimens

3.5.2. Strengthening of specimens

The process of strengthening reinforced concrete beams with fiber reinforced polymer (FRP) sheets involves several steps. The first step was to prepare the concrete beam by grinding and cleaning the surface as shown in Fig. 18-a. This helps to create a good bond between the concrete and the FRP sheets. Next, the beams were marked in the places of the FRP sheets and FRP anchors holes (Fig. 18-b). The holes were then drilled at the marked locations using a drill bet that has the same size as the desired hole as shown in Fig. 18-c Then, FRP sheets were cut to the appropriate size and shape (Fig. 18-d). Before strengthening the beam, it is important to ensure that it is clean, dry, and free of any debris or defects that could affect the performance of the FRP sheets. Therefore, the beams and the holes were cleaned thoroughly using a vacuum cleaner

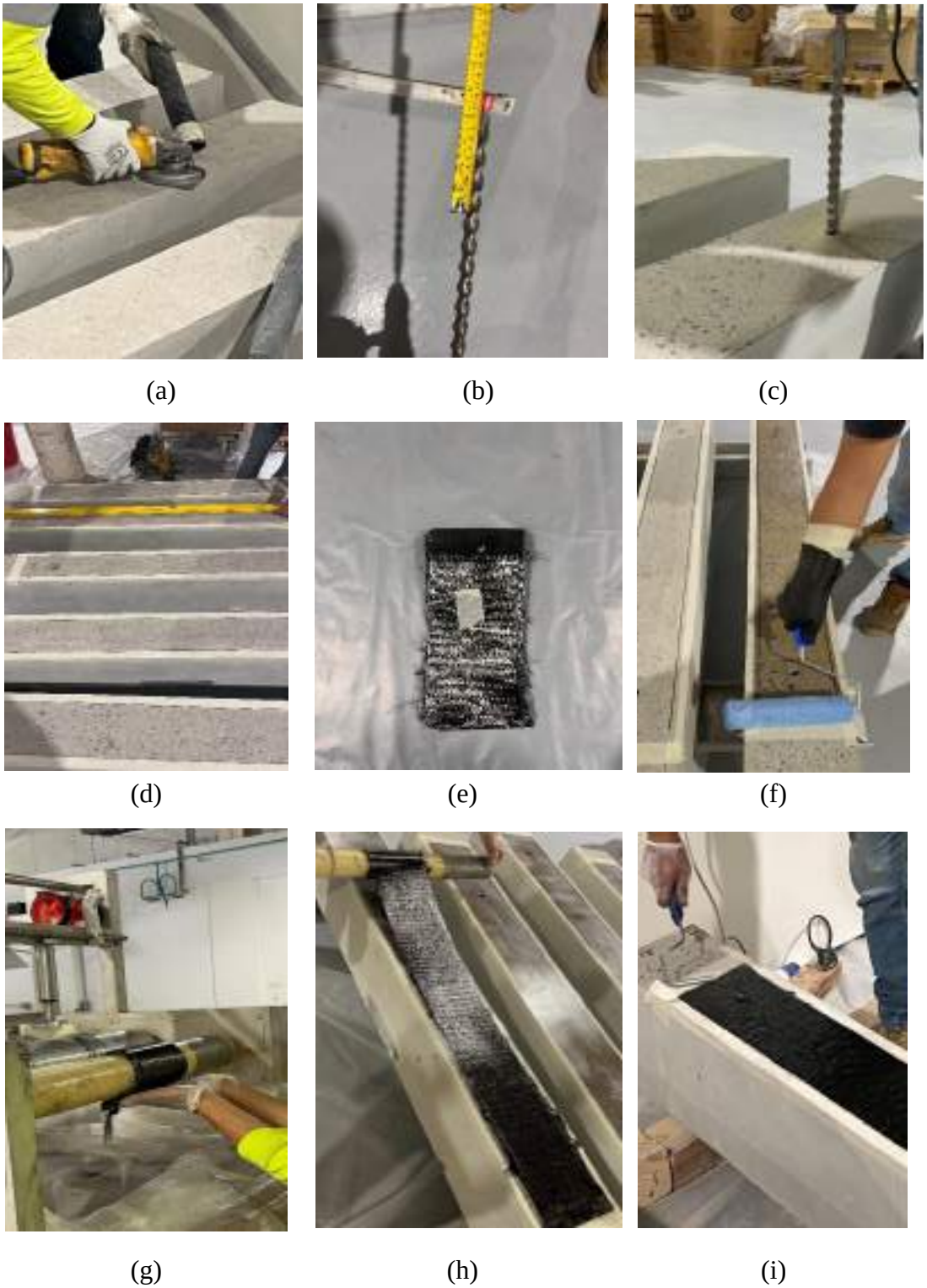

(a) (b) (c)

(d) (e) (f)

(g) (h) (i)

Figure 18: Strengthening procedure

and a towel. After that, a layer of primer was applied to the beams using a roller (Fig. 18-d) and then the epoxy paste layer was applied. The primer was created by combining the two-part epoxy adhesive (V-WrapTM770) [79] in the ratio of 2:1, as recommended by the manufacturer. The epoxy paste was created by mixing fumed silica with a portion of the primer mixture. Finally, the CFRP sheets were impregnated with primer using the tool shown in Fig. 18-e and then the sheets were attached to the concrete surface. To eliminate any potential air voids in the CFRP laminates, grooved rollers were used as in Fig 18-i.

The preparation of FRP anchors involves cutting the CFRP sheets according to the required length and width (diameter) of the CFRP anchor. The fibers composing the CFRP sheets are then released and regrouped together to form the desired FRP anchor diameter. The length of the sheet equals the embedment depth plus the fan length of the anchor, and this equals the total length of the FRP anchor. Prior to installing FRP anchors in the beams, the holes were cleaned and impregnated with primer as illustrated in Figs. 19-a, and 19-b. The anchors were also impregnated well with primer as (Fig. 19-c). Primer was then applied using grooved rollers over the fan length to spread it out on the CFRP sheet Fig. 19-d. Finally, a layer of epoxy was applied over the fan and in in the hole to fill any gaps left (Fig. 19-e and Fig. 19-f) . Some of the anchored specimens are shown in Fig. 20.

(a)

(b)

(c)

(d)

(e)

(f)

Figure 19: Anchors installation

(a) Prepared FRP anchor (Ø14 mm)

(b) Specimens with 2 anchors (Ø20 mm) and 4 anchors (Ø14 mm)

(c) Some of the prepared specimens

Figure 20: Strengthened and anchored specimens

Chapter 4. Experimental Program

This chapter presents the experimental results of seventeen tested beams. The experimental results are in the form of failure modes, load-deflection responses, strain measurements, and maximum obtained strengths and deflections.

4.1. Failure Modes

In this study, all beams were designed to fail in flexure. The most dominant failure mode in the strengthened specimens was delamination, i.e., the concrete cover separates at the end of the specimens as summarized in Table 5. Anchor failure was observed in few specimens. Figs 21-27 show the failure mode of each tested beam.

Despite that delamination or debonding has occurred in all of the anchored specimens, it can be observed that the concrete cover layer remained intact with the beam specimen in almost all of the anchored beams except for the beams having inclined anchors (Fig. 27) The concrete cover layer was totally separated in these specimens, similar to the unanchored one. An obvious separation can also be seen in specimen (A22-H140-F220), which experienced anchor pullout. This specimen had a lesser anchor embedment depth and fan length which indicates the importance of having sufficient depth and length for the purpose of utilizing the anchor's function in delaying the delamination failure. Anchor rupture was observed in specimen (A14-H100-F180). Concrete crushing can be observed in some specimens. However, crushing occurred after delamination initiated since the anchored beams remained intact, although loading started to drop down.

Table 5: Summary of failure modes

Group No.	**Specimen**	**Failure mode**
1	B	Concrete crushing after steel yielding
	BU	Delamination
2	A14-H80-F180	Debonding
	A14-H80-F120	Delamination
	A14-H100-F180	Debonding + anchor rupture
3	4A14-H100-F180	Debonding

	4A14-H80-F120	Debonding
4	A20-H120-F260	Delamination
	A20-H100-F260	Delamination
5	A22-H140-F280	Delamination
	A22-H160-F280	Delamination
	A22-H140-F220	Delamination + anchor pullout
6	A24-H150-F300	Delamination
	A24-H120-F300	Delamination
	A24-H150-F260	Delamination
7	IA14-H100-F180	Delamination
	IA20-H100-F260	Delamination

It can be seen from Fig. 21-a that the control beam has failed in flexure. The failure started with cracking on the tension side of the beam, and as the load increased, the cracks widened and propagated until the concrete crushing occurred at the compression side. At this stage, reinforcing bars have yielded. Fig. 21-b shows the flexure-shear delamination failure of BU specimen. As expected, cracks were formed near the end of the FRP sheet. Then, the cracks propagated along the level of the steel reinforcement which resulted in the separation of the concrete cover.

(a) Control beam (B)

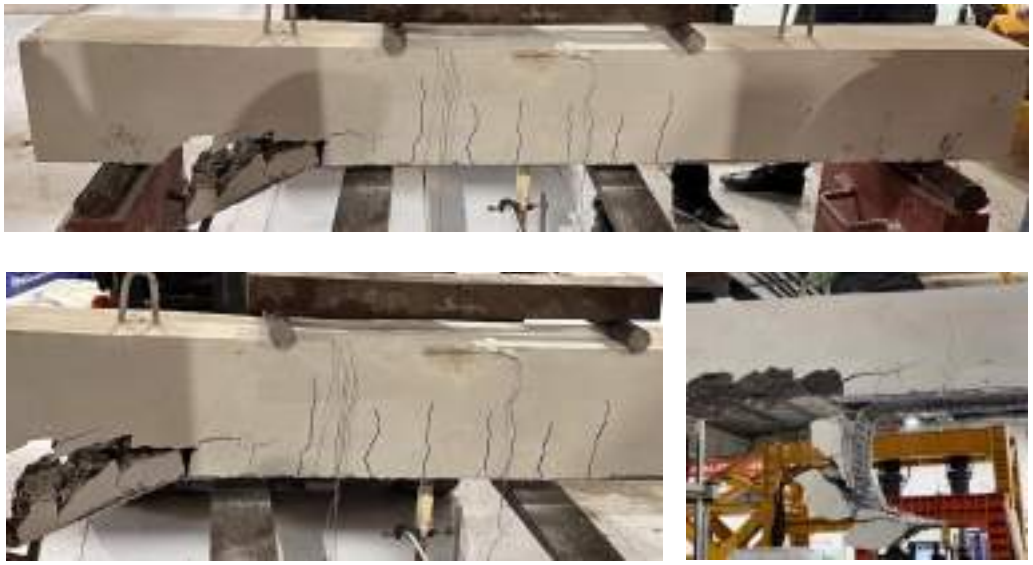

(b) Strengthened unanchored beam (BU)

Figure 21: Failure mode of group 1 beams

Fig. 22 (a-c) shows the failure of the beam specimens anchored with one anchor of diameter 14 mm on each side. The first beam (A14-H80-F120) was failed by delamination on one side. However, the failure is quite different than the BU beam. It can be seen that the concrete cover layer was not totally separated from the rest of the beam. This indicates that the anchor has held the concrete cover with the upper part of the beam and prevented it from the total separation. The second and third beams of this

(a) Specimen A14-H80-F120

(b) Specimen A14-H80-F180

(c) Specimen A14-H100-F180

Figure 22: Failure mode of group 2 beams

group (A14-H80-F180 and A14-H100-F120) were failed by debonding of the CFRP sheet from the concrete substrate. The failure of the third beam was also accompanied by rupture of the anchor which can be seen in Fig. 22-c. Concrete crushing can be observed in Fig. 23-a and 25-a. Nonetheless, the crushing of concrete has occurred way after the debonding failure. By then, the load has significantly dropped.

The third group demonstrated excellent behavior in terms of the failure patterns. Fig. 23-a and 23-b show that debonding took place in both beam specimens. The difference between this debonding failure and the debonding that occurred in the previous group is that the FRP sheet remained connected to the concrete with the help

of the FRP anchors. Thus, the existence of two FRP anchors on each side improved the failure behavior of strengthened beams.

(a) Specimen 4A14-H80-F120

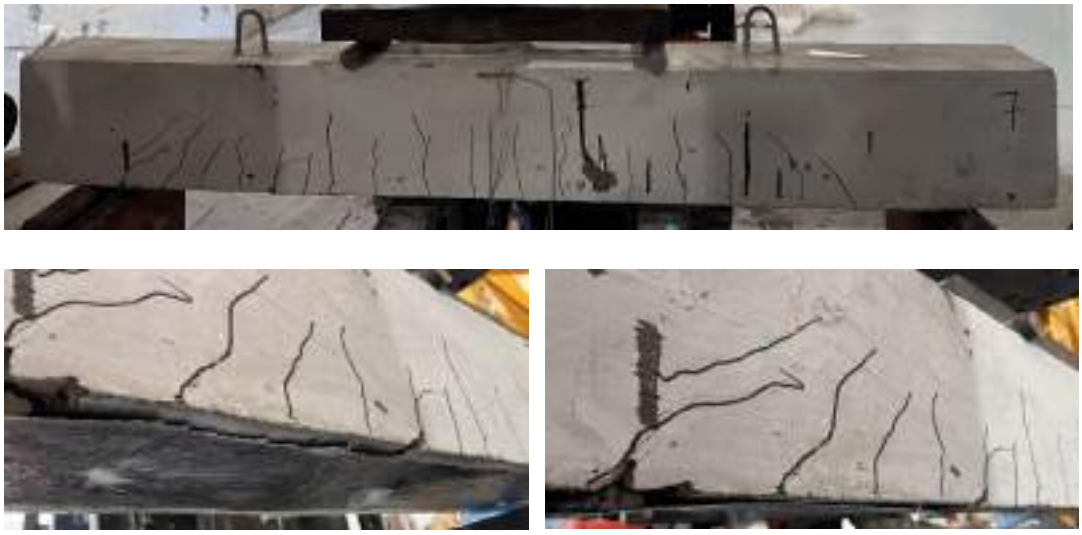

(b) Specimen 4A14-H100-F180

Figure 23: Failure mode of group 3 beams

A typical failure in the form of delamination for beams anchored with 20 mm diameter anchors can be seen in Fig. 24-a and 24-b. Specimen A20-H120-F260 (with a higher embedment depth) examined a better failure behavior, although the ultimate load it could bear was less, as will be discussed later. A more improved failure behavior is depicted in specimens A22-H140-F280 and A22-H160-F280 of Group 5 in Fig. 25-a and 25-b. The flexure-shear delamination cracks can be noticed near the sheet's end

and along the concrete cover, but no clear separation of the concrete cover occurred. On the other hand, specimen A22-H140-F220 experienced anchor pullout failure which resulted in severe detachment of the concrete cover. This can be attributed to either an insufficient embedment depth or fan length. It could also develop due to not filling the anchor hole fully with primer and epoxy, which results in a weak bond between the FRP anchor and the surrounding concrete.

(a) Specimen A20-H100-F260

(b) Specimen A20-H120-F260

Figure 24: Failure mode of group 4 beams

(a) Specimen A22-H140-F280

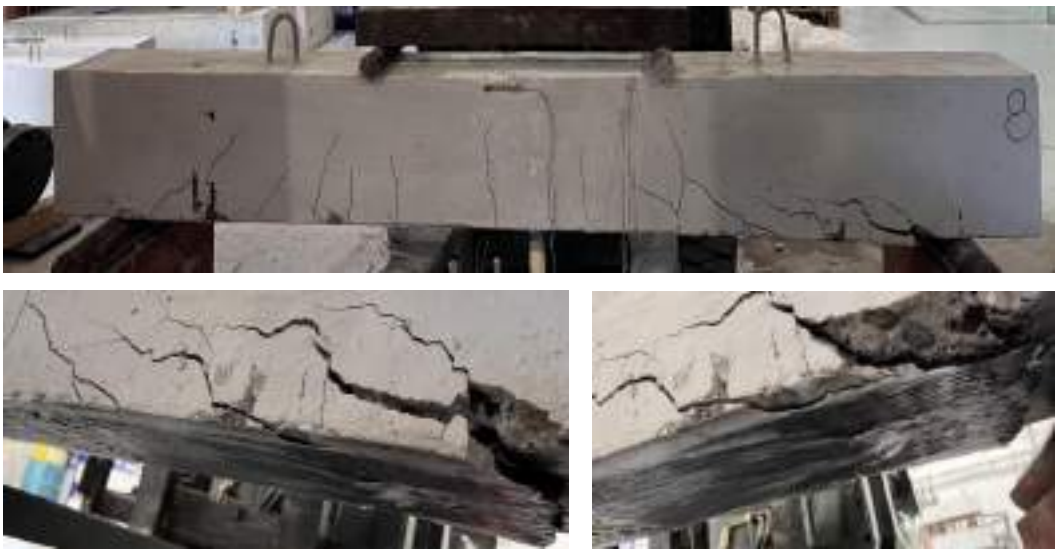

(b) Specimen A22-H160-F280

(c) Specimen A22-H140-F220

Figure 25: Failure mode of group 5 beams

Fig. 26 (a-c) shows the failure of Group 6 specimens, anchored with diameter 24 mm. Similar to the behavior of previous groups, the beam anchored with a higher embedment depth and fan length (A24-H150-F300) examined a superior failure behavior compared to its counterparts in the same group. The failure of beams having an inclined anchor at a 45° are shown in Fig. 27. Clearly, the beams have encountered an undesirable response at failure in the form of complete separation of the concrete cover from the end of the beam until almost the middle of it. The failure of this group was even more critical than the unanchored beam.

(a) Specimen A24-H120-F300

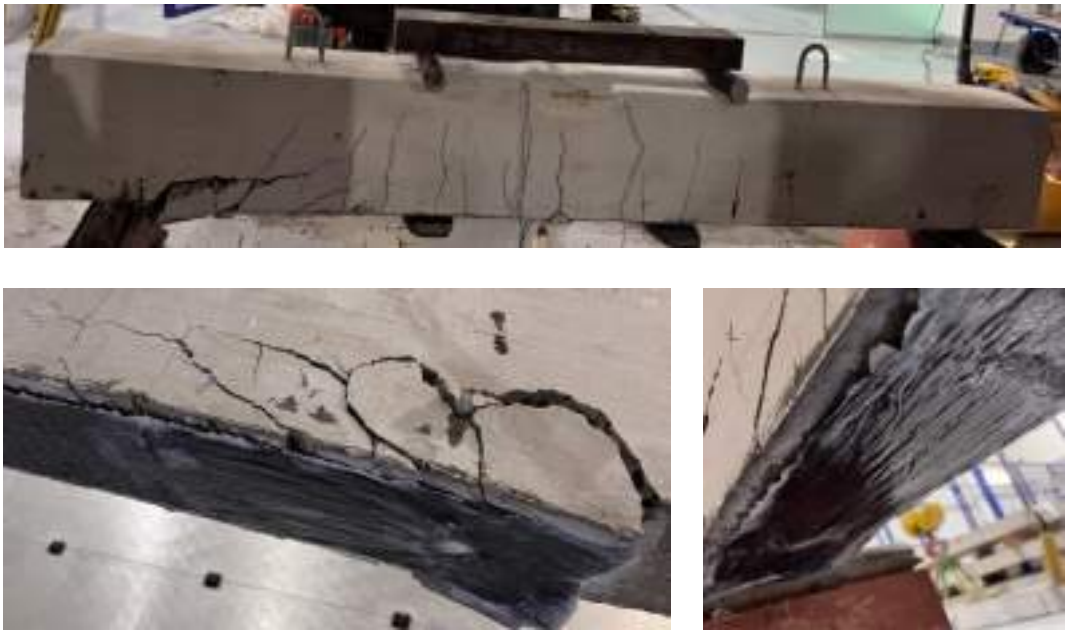

(b) Specimen A24-H150-F260

(c) Specimen A24-H150-F300

Figure 26: Failure mode of group 6 beams

(a) Specimen IA14-H100-F180

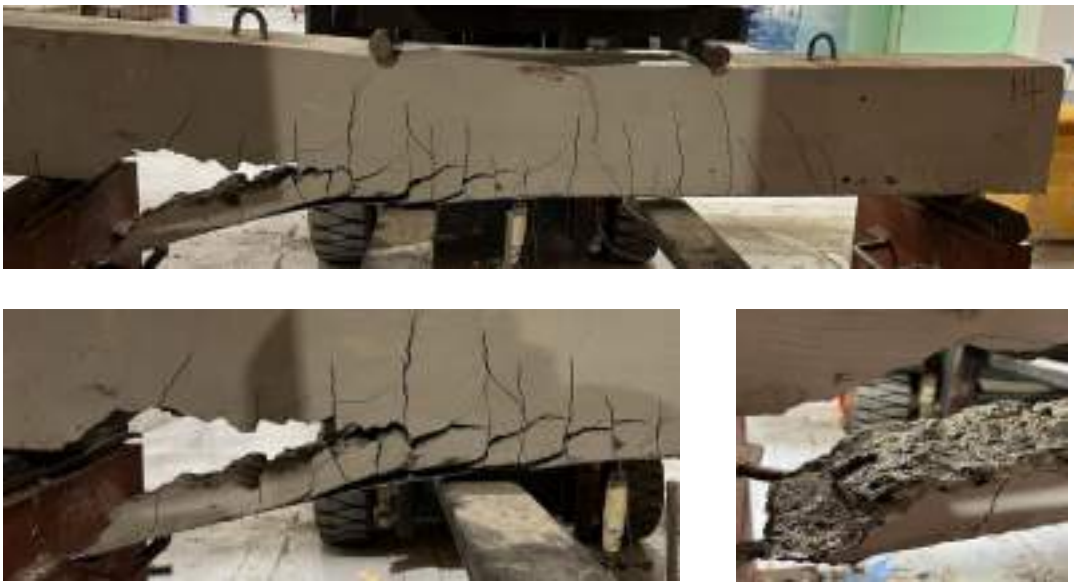

(b) Specimen IA20-H100-F260

Figure 27: Failure modes of group 7 beams

4.2. Strain in Flexural Steel Reinforcement and Concrete

Load-strain measurements of the constituent materials of RC beams provide valuable insights into the behavior of the beam under load. As mentioned earlier, concrete and steel strain gauges were installed at the beams' midspan. Figs. 28-34 show the load-strain responses in the concrete and steel reinforcement for each group. Evidently, none of the tested specimens has reached the maximum usable compression strain in concrete, which is 3000 με. Therefore, none of the tested beams failed by concrete crushing. Looking at the load-strain plots of reinforcing steel, it can be observed that all beams reached the yielding strain (2800 με) before reaching the ultimate load. This means that yielding of steel reinforcement has occurred before the debonding or delamination in any of the strengthened beams. It should be noted that

some strain recordings for steel bars did not reach the ultimate load. This could be due to a malfunction that may occurred to the strain gauges during higher loadings.

Generally, the strain values of steel reinforcement at failure loads in the anchored beams are higher than the control beam with a range of increase between 20 to 70%. This indicates that anchoring the CFRP laminates delayed the debonding failure and utilized more of the steel strain. However, two anchored beam specimens showed

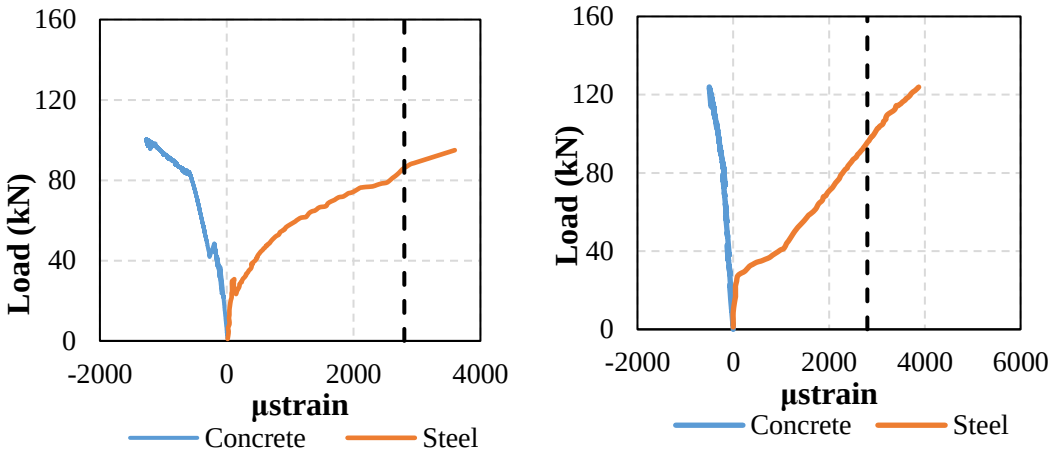

(a) B (b) BU

Figure 28: Strain measurements of concrete and steel for Group 1 beams

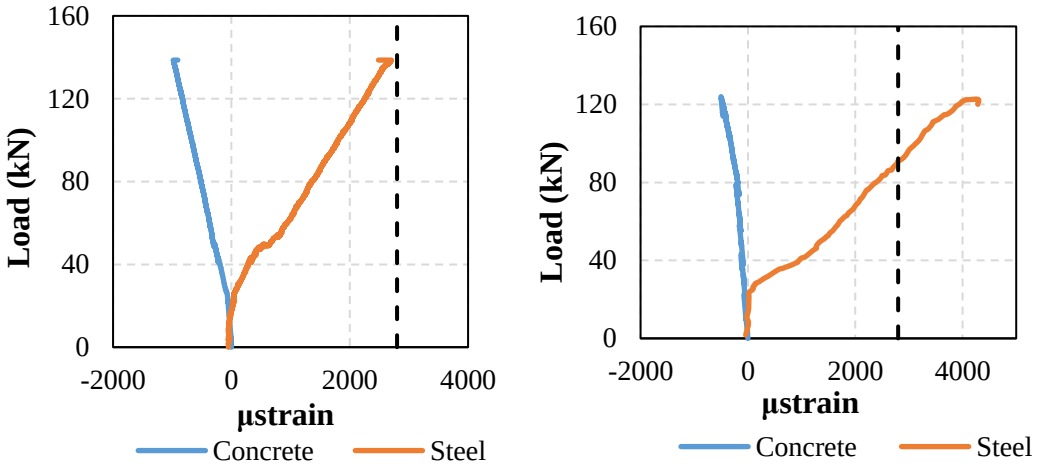

(a) A14-H80-F120 (b) A14-H80-F180

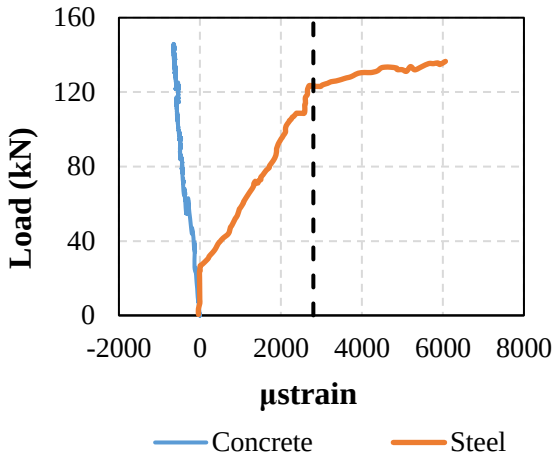

(c) A14-H100-F180

Figure 29: Strain measurements of concrete and steel for Group 2 beams

lower strain values in the steel compared to the control beam. These beam specimens (A14-H80-F120 and A24-H150-F260) have also exhibited much lower strains in the CFRP laminates as will be seen in the proceeding section, indicating that the premature delamination occurred way before utilizing the beam's capacity.

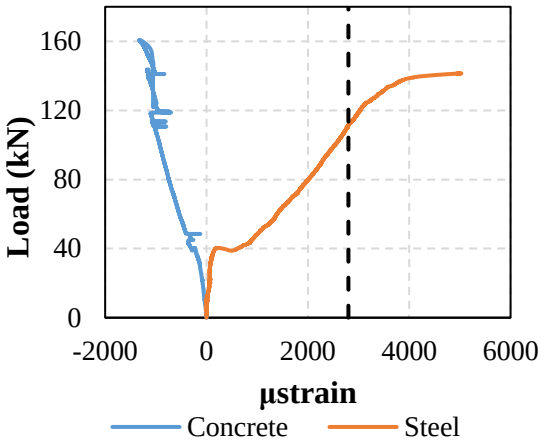

(a) 4A14-H100-F180

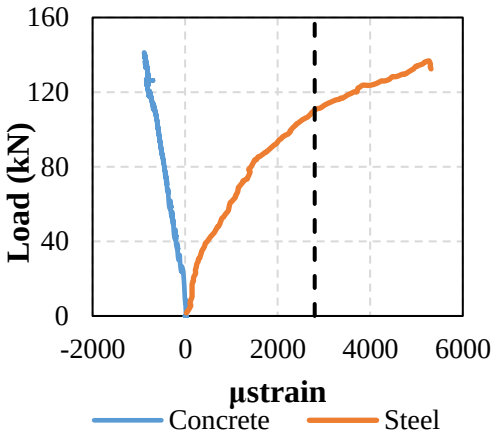

(b) 4A14-H80-F120

(b) Figure 30: Strain measurements of concrete and steel for Group 3 beams

It can be seen from Fig. 30 that specimen A14-H100-F180 exhibited the highest value in the strain of the steel reinforcement among the group specimens. This conveys that this specimen utilized more of the steel strain which agrees with the load-deflection

behavior and the FRP strain measurements of this specimen, as will be shown in the proceeding sections.

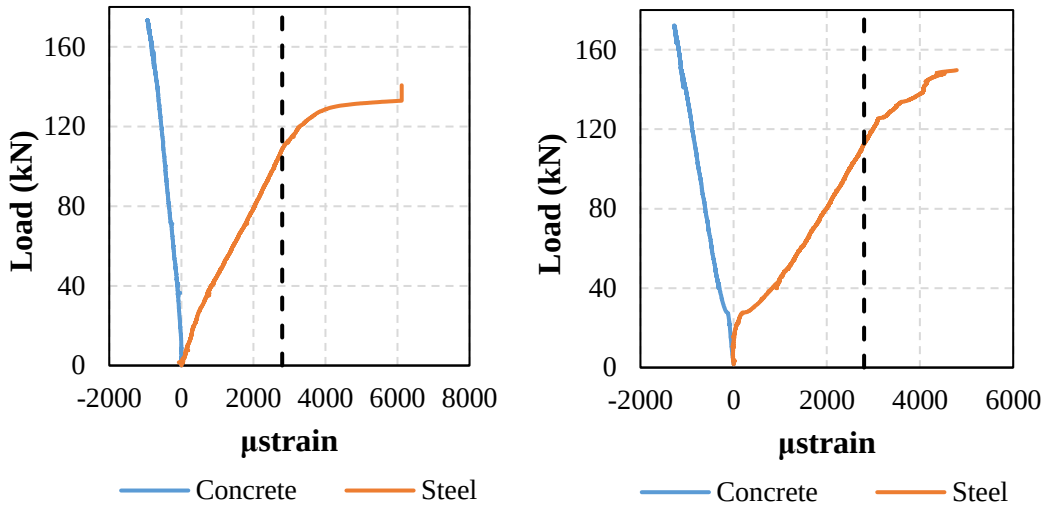

(a) A20-H100-F260 (b) A20-H120-F260

Figure 31: Strain measurements of concrete and steel for Group 4 beams

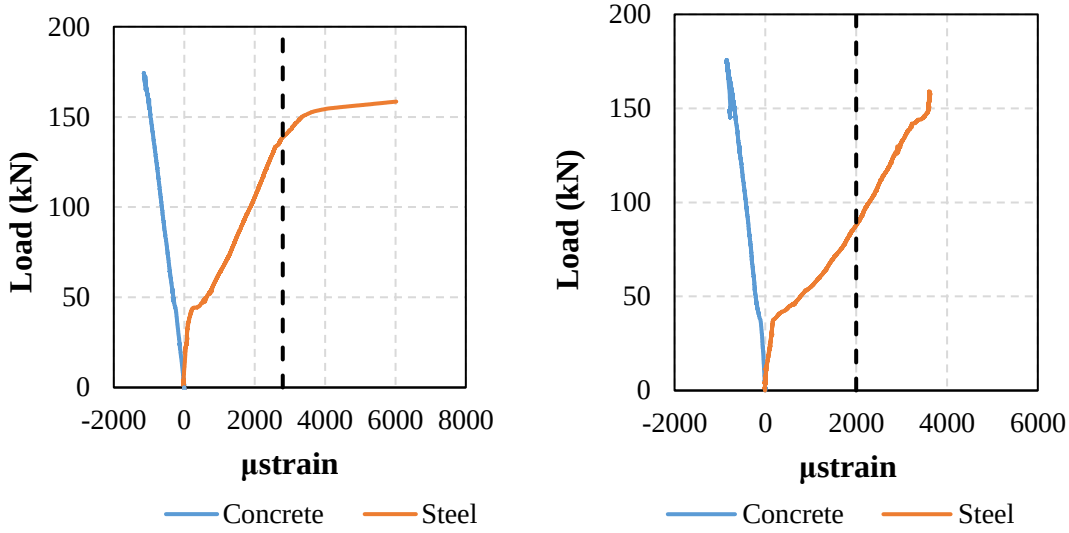

(a) A22-H140-F220 (b) A22-H140-F280

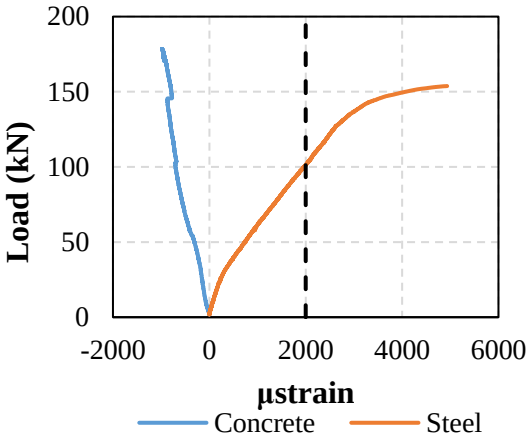

(c) A22-H160-F280

Figure 32: Strain measurements of concrete and steel for Group 5 beams

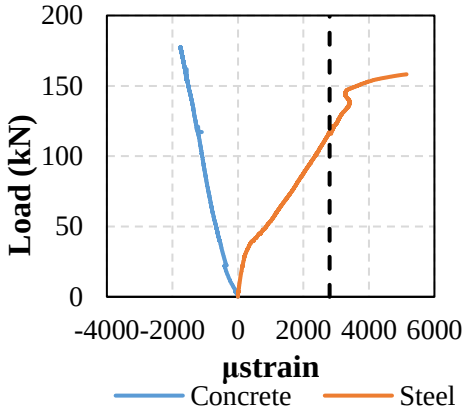

(a) A24-H120-F300

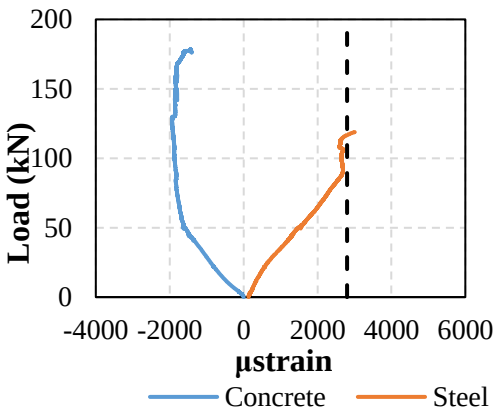

(b) A24-H150-F260

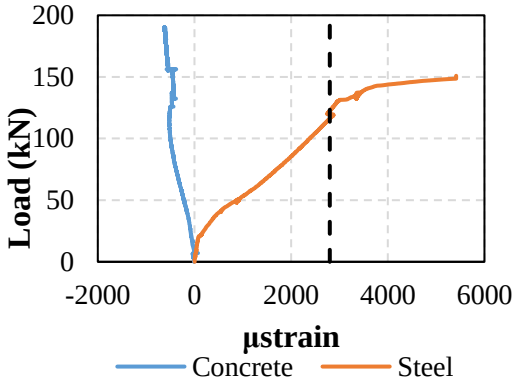

(c) A24-H150-F300

(d) Figure 33: Strain measurements of concrete and steel for Group 6 beams

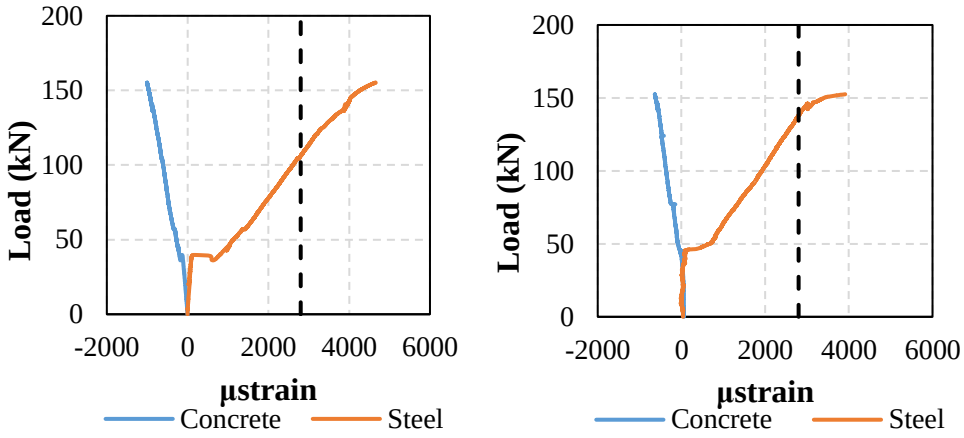

(a) IA14-H100-F180 (b) IA20-H100-F260

Figure 34: Strain measurements of concrete and steel for Group 7 beams

4.3. Load-Deflection Curves

The load deflection curves are important tools for analyzing the behavior of beams under flexure. The load versus midspan deflection of all tested beams is shown in Figs. 35-41. Each group specimens' plots are compared to the control unstrengthened and the unanchored beam, respectively. The load values were taken from the Instron UTM machine, and the displacement values were obtained from the LVDT placed at the midspan of the beam, as mentioned previously.

As illustrated in Figs. 35-41, the load-deflection curve of the control specimen (B) shows a typical behavior of a RC beam under loading. It consists of two distinct regions: the linear-elastic region and the nonlinear region. In the linear-elastic region and prior to cracking, the beam undergoes a small amount of deflection in response to the applied load. The elastic stiffness of all beams in this region is similar as can be seen in Figs. 36-42. The relationship between the load and deflection remains linear up until the yielding point with a decrease in the flexural stiffness due to a drop in the moment of inertia of the cracked sections in all specimens. In this phase, the strengthened beams have a 30% higher elastic stiffness compared to the control beam. Also, this stiffness is similar for all the strengthened (whether anchored or unanchored) beams.

The non-linear region of the control beam's load-deflection curve is characterized by a gradual loss of strength and stiffness as the beam approaches failure. After reaching its ultimate limit state at a load of 100.3 kN, the load-deflection curve had a sharp drop in load at a maximum deflection of 29.3 mm. A 10% and 24% increase in yield load and ultimate load are depicted in the strengthened unanchored specimen (BU) compared to the control beam (B), respectively. After reaching the ultimate state, the load showed a sudden drop at a maximum deflection of 10.1 mm. This implies that flexural strengthening with CFRP laminates enhanced the strength but significantly reduced the ductility of the RC beam which resulted in a brittle failure.

Regarding anchored specimens with a 14-mm diameter anchors (Group 2), a slight increase in the ultimate load is portrayed by specimen A14-H80-F120 (12%) compared to specimen BU, with a negligible increase in the maximum deflection as shown in Fig. 35. A more desirable behavior is presented by the other two specimens in the group with an enhancement in the ultimate load of 17% and 18% for A14-H80-F180 and A14-H100-F180, respectively. Though sample A14-H80-F120 had almost the same deflection as the unanchored beam (10.7 mm), the other two beams showed an increase of 66% and 38% in maximum deflection for A14-H80-F180 and A14-H100-F180, respectively.

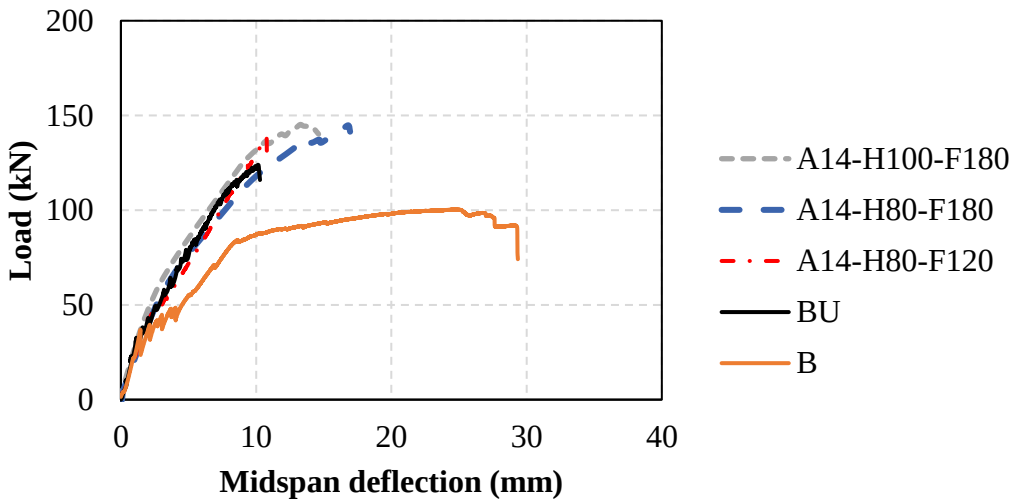

Figure 35: load-deflection curve for Group 2 specimens

The effect of increasing the number of anchors at each end was studied in Group 3 as shown in Fig. 36. For the same embedment depth and fan length, adding one anchor at each end did not increase the ultimate capacity of the beam. In fact, the beam having only two anchors (A14-H80-F120) showed higher flexural capacity compared to the one that has four anchors (4A14-H80-F120). Nevertheless, maximum strain value in the CFRP laminates of 4A14-H80-F120 specimen was very close to the rupture strain of CFRP as will be demonstrated in the next section. Specimen 4A14-H100-F180 achieved the highest ultimate load with a percentage increase of 30% beyond BU and 60% beyond B.

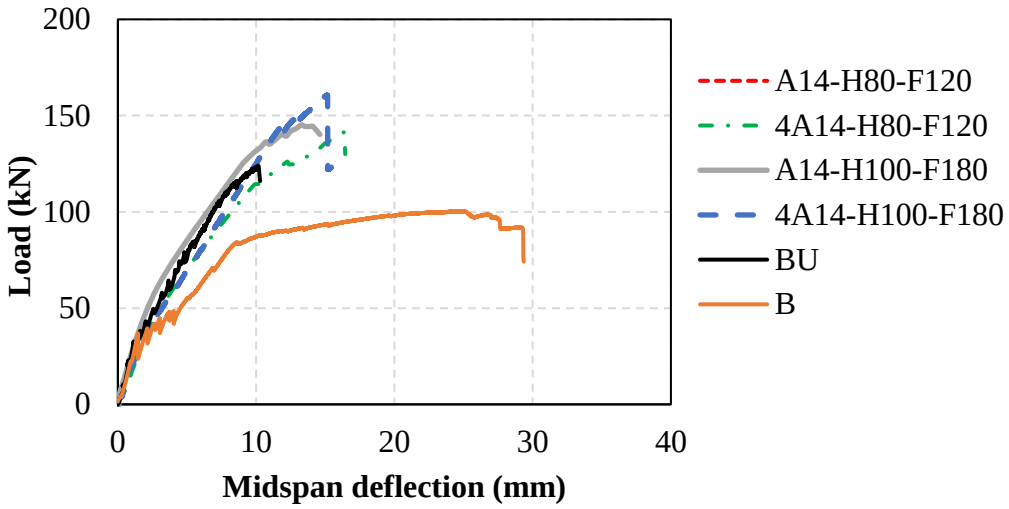

Figure 36: Load-deflection curve for Group 3 specimens

Group 3 specimens include beams anchored with 20 mm diameter anchor at each end. the difference between the two beams is in the embedment depth. As depicted in Fig. 37, the two specimens (A20-H100-F260 and A20-H120-F260) exhibited a quite similar behavior with an increase in the ultimate load of (39-42%) compared to the unanchored beam and a percentage increase of (72-75%) compared to the unstrengthened control beam. Anchors with larger diameter (22 and 24 mm) were investigated in group 5 and group 6, respectively. A similar trend is detected here in Figs. 38 and 39 where increasing the embedment depth and fan length resulted in a slight increase of the ultimate load-carrying capacity. Primarily, beam specimens anchored with larger diameter showed superior flexural response compared to beams anchored with smaller dowel diameters. In fact, specimen A24-H150-F300 featured a

percentage increase in the maximum load of 90% and 53% beyond specimens B, and BU, respectively.

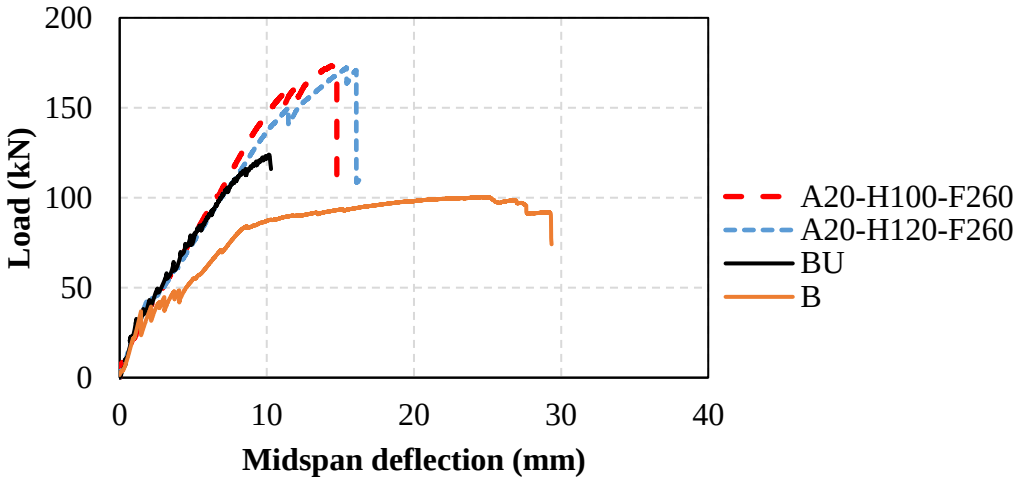

Figure 37: Load-deflection curve for Group 4 specimens

Fig. 40 shows the influence of the angle of inclination of anchor's dowel on the behavior of anchored beams. A negligible difference is noted between vertical and inclined anchors of diameter 14 mm. For anchors of diameter 20 mm, the beam specimen with a vertical anchor showed a superior behavior as opposed to the beam having inclined anchors with 45° angle. Moreover, the failure behavior of both beams having an inclined anchor was undesirable where a sudden and complete separation of the concrete cover occurred which is considered a brittle failure as discussed in the previous section.

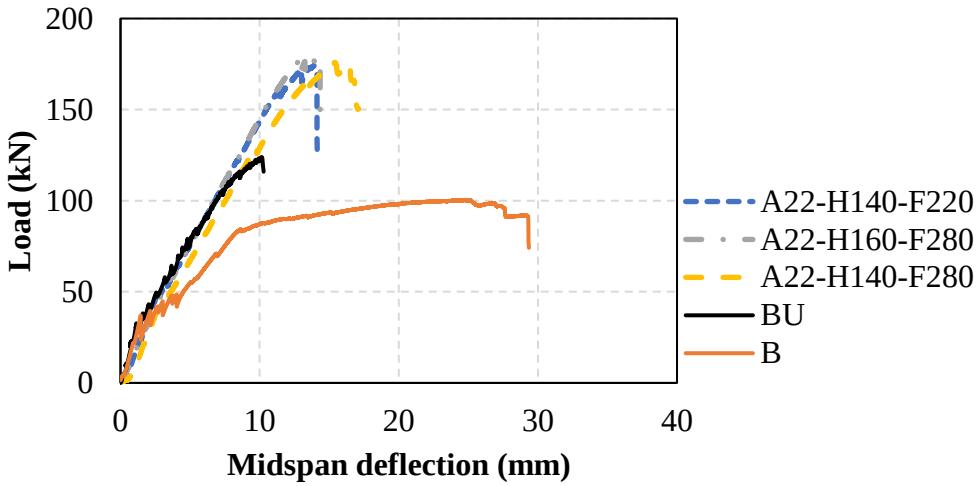

Figure 38: Load-deflection curve for Group 5 specimens

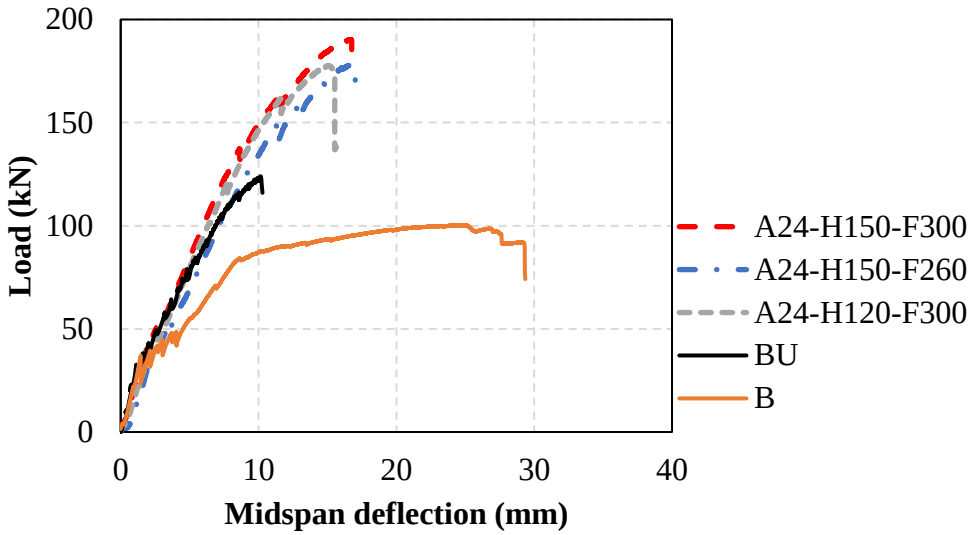

Figure 39: Load-deflection curve for Group 6 specimens

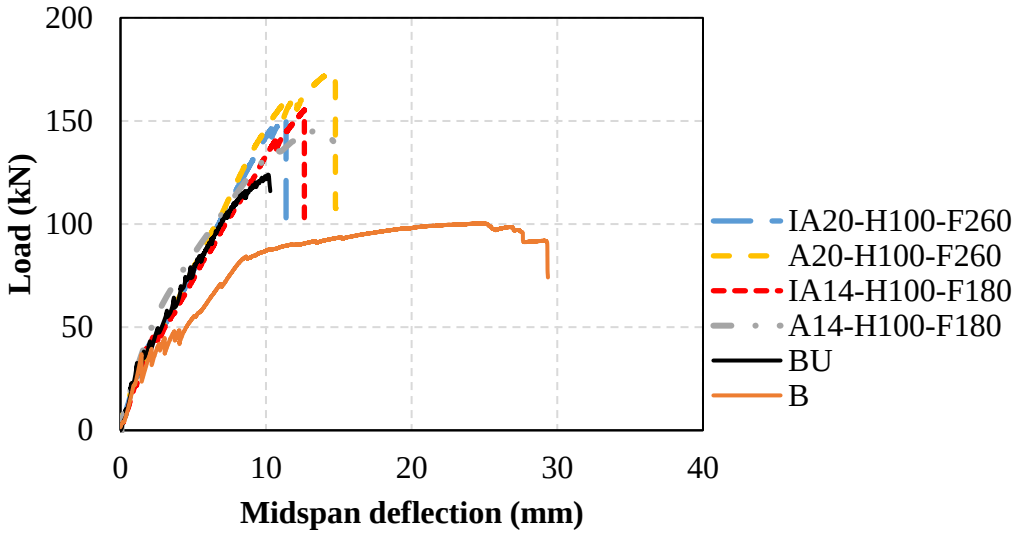

Figure 40: Load-deflection curve for Group 7 specimens

4.4. Strain measurements in the CFRP laminates

To evaluate how anchorage affects the utilization level of CFRP ultimate strain, it was crucial to measure the strains present in the CFRP laminates. For this purpose, two strain gauges were affixed on the CFRP laminate at the midspan of each strengthened beam. to simplify, the values of the strain gauge with the higher reading

are reported herein. The load versus CFRP strain for each beam specimen was plotted and presented in Figs. 41-48. Initially, the strains in the CFRP laminates are very small. Post cracking, CFRP laminates started to engage in taking the load. This can be noted in the load-strain plots by a change in the slope of the curve at a load of about 20 to 40 kN. The curve then ascends until failure occurs in the strengthened beam where a sudden drop or a leap takes place. In the load-strain figures below, the curve was stopped at the point where failure occurred.

Fig. 41 displays the load-strain curves for all strengthened specimens. A prominent increase in the maximum strain in the anchored specimens is noticed. It is also apparent that the specimens with four anchors presented the highest values of CFRP strain although they did not exhibit the highest ultimate load. Specimen 4A14-H100-F180 had a maximum strain in the CFRP laminate of 10900 με, very close to the rupture strain of CFRP which is 11000 με. This marks a significant improvement in utilizing the strain of FRP laminates by means of anchorage.

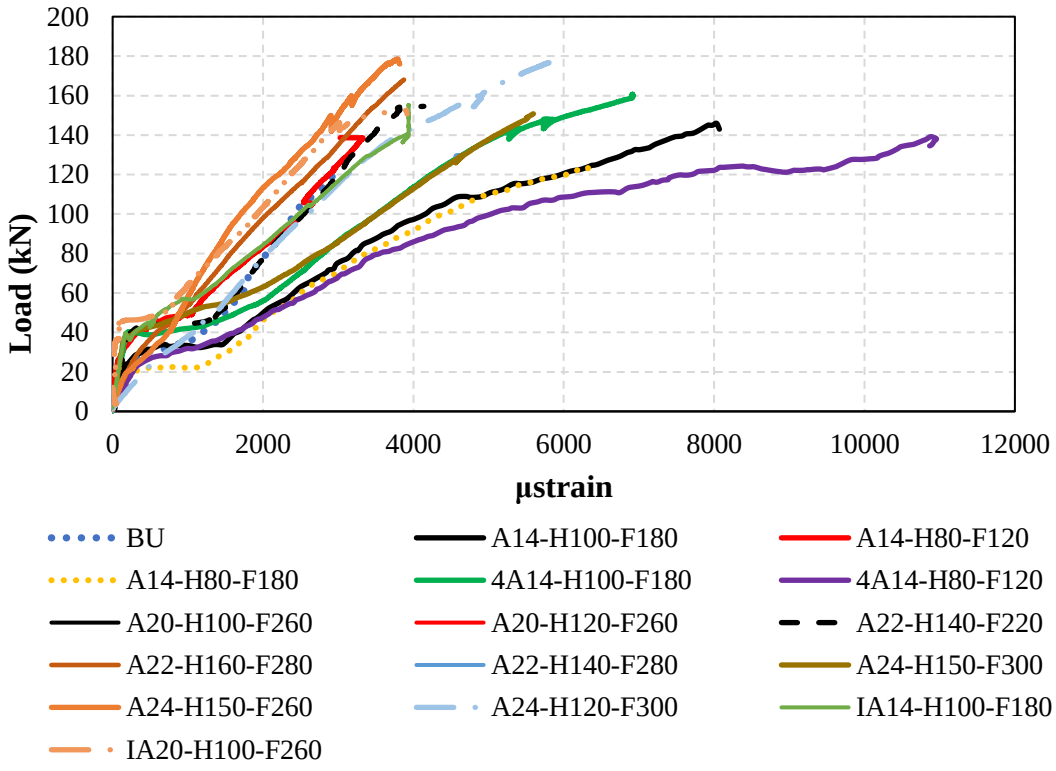

Figure 41: Load-strain curves of all strengthened specimens

Fig. 42 shows the load-strain plots of group 2. The slope of load strain curve of the two specimens having a higher fan length is almost similar (A14-H100-F180 and A14-H80-F180). However, A14-H100-F180 featured a maximum strain of 8066 με compared to a strain of 6687 με, shown by specimen A14-H80-F180. A14-H80-F120 had an undesirable value of the maximum attained strain, which was equal to 3329 με. As mentioned earlier, group 3 specimens showed a superior behavior in terms of the maximum strain in the CFRP laminates. The load-strain curves for 4A14-H80-F120 and 4A14-H100-F180 are illustrated in Fig. 43.

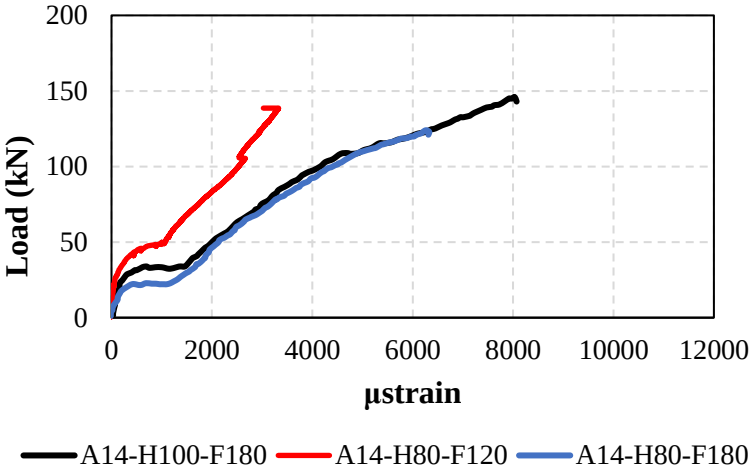

Figure 42: Load-strain curves of CFRP for Group 2 specimens

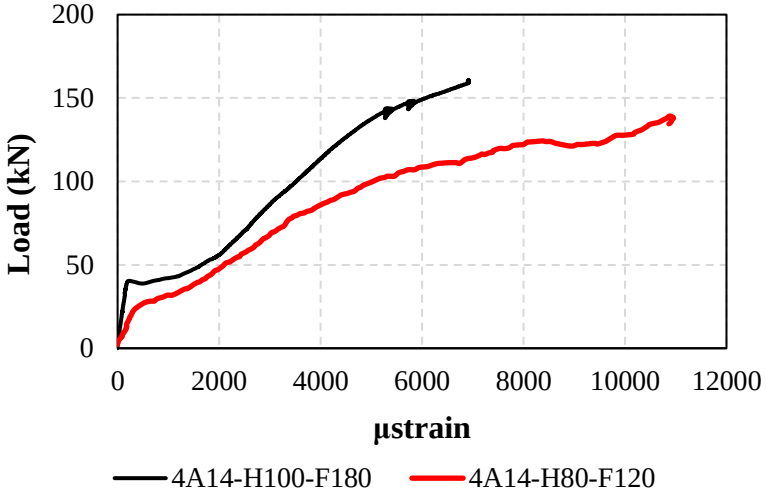

Figure 43: Load-strain curves of CFRP for Group 3 specimens

Specimens A20-H100-F260 and A20-H120-F260 had almost identical load-strain curves as shown in Fig. 44. However, the maximum strain by the later specimen

surpassed the former by 7%. Group 5 and Group 6 specimens show a similar trend, in which the specimen with the lesser embedment depth and higher fan length achieved a higher maximum strain in the CFRP as depicted by Figs 45 and 46. A slight increase in the load and the slope of the load-strain curve is noticed for the specimens that achieved less maximum strain in the CFRP. Nonetheless, Group 7 specimens had almost the same ultimate load as shown in Fig. 48, but with a 38% increase in the maximum strain attained by specimen IA20-H100-F260.

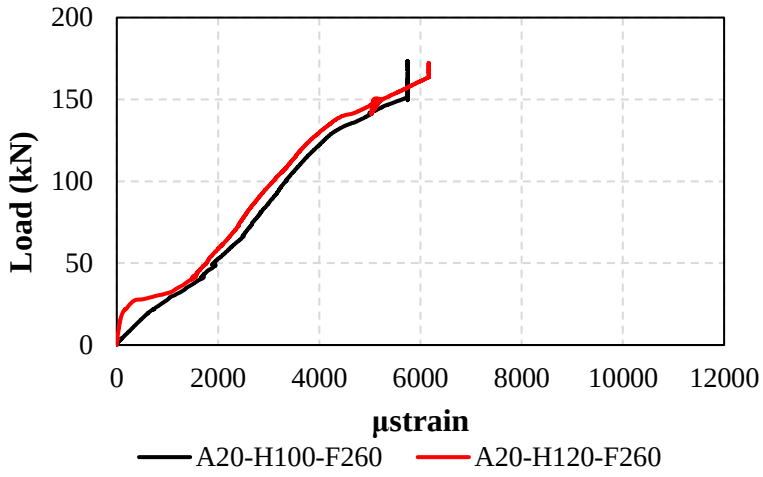

Figure 44: Load-strain curves of CFRP for Group 4 specimens

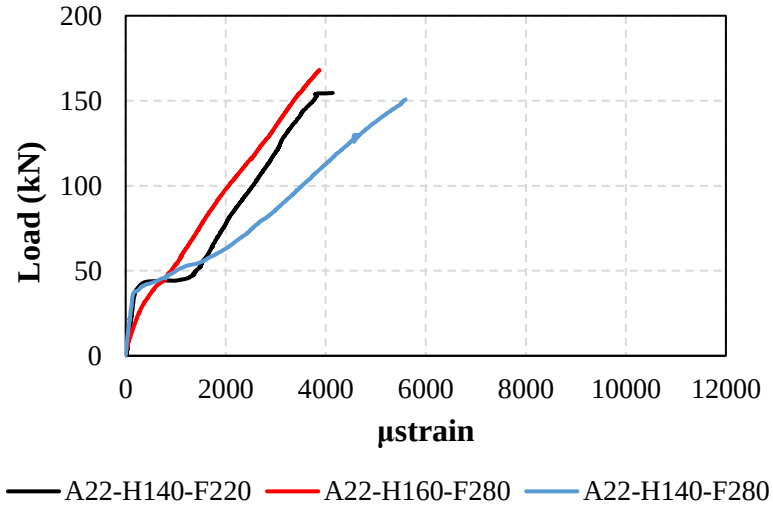

Figure 45: Load-strain curves of CFRP for Group 5 specimens

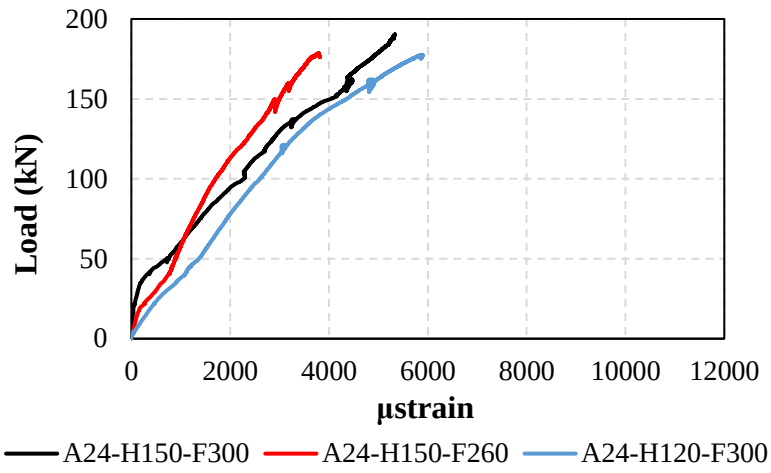

Figure 46: Load-strain curves of CFRP for Group 6 specimens

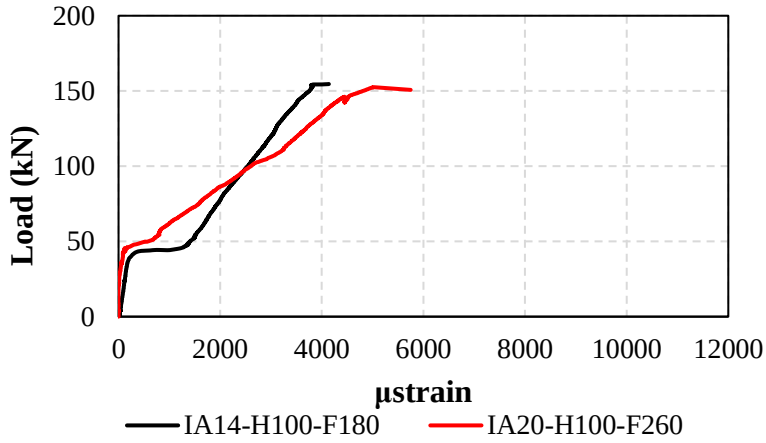

Figure 47: Load-strain curves of CFRP for Group 7 specimens

Chapter 5. Discussion of Results

This chapter presents and discusses the experimental results in terms of flexural strength and ductility. The anchored specimens are evaluated in relation to the unstrengthened specimen and unanchored specimens. Furthermore, the flexural capacity and ductility are compared between specimens in each group.

5.1. Flexural Strength

A summary of the test results in terms of yield strength, ultimate and final strength, and their corresponding midspan deformation is presented in Table 6. To have a more valuable insight into the effectiveness of each anchorage scheme, the percentage increase in the ultimate load with respect to the control unstrengthened and the unanchored beams were calculated and presented in Fig. 48, respectively. In addition, the percentage of strain utilization is illustrated in Figs. 49. The results reported in this section are thoroughly discussed and analyzed in the following subsections.

5.1.1. Effect of strengthening

It was revealed from the presented results that strengthening RC beams with CFRP laminates enhanced the flexural capacity and significantly increased the stiffness of the strengthened beam. Strengthening without anchors lead to a percentage increase in the ultimate load of 24% compared to the control beam as shown by Fig. 48. However, a brittle failure for the unanchored beam was reported in the form of sudden concrete cover separation which prevented the utilization of the full strengthened beam flexural capacity. From Fig. 49, it is discernible that the maximum attained strain in the CFRP laminates was only 27% of the CFRP rupture strain.

5.1.2. Effect of anchorage

Anchorage of the CFRP laminates using CFRP splay anchors resulted in a noticeable improvement in the flexural behavior of strengthened RC beams. Fig. 48 illustrates the extent of enhancement in the ultimate load carrying capacity with respect to the unstrengthened and unanchored beams. All anchored beams exhibited a higher percentage increase in the flexural strength compared to the unanchored beam. The ultimate load surged in the range of 12% to 53% in comparison with the unanchored specimen. It can also be shown that the level of strain utilization ($\varepsilon_{ult}/\varepsilon_{rup}$) for all

anchored specimens exceeded the counterpart value of the unanchored beam. In addition, the behavior of the majority of the anchored beams at failure was more favorable than the unanchored one. Although the failure was in the form of delamination, the anchors prevented the complete and abrupt separation of the concrete cover.

Table 6: Summary of the test results

Designation	P_y (kN)	δ_y (mm)	P_u (kN)	δ_u (mm)	P_f (kN)	δ_f (mm)	ε_{ult}
B	86.70	9.88	100.28	24.65	91.30	29.29	-
BU	95.80	6.49	123.97	10.12	99.17	10.12	0.003013
A14-H80-F120	108.2	10.70	138.60	10.70	110.88	10.70	0.003329
A14-H80-F180	90.96	6.75	144.63	16.76	115.70	9.60	0.008135
A14-H100-F180	123.50	8.67	145.95	13.95	116.76	13.95	0.008066
4A14-H80-F120	110.53	9.44	141.30	16.49	113.04	16.49	0.010905
4A14-H100-F180	111.44	8.77	160.63	15.11	12.09	15.11	0.006916
A20-H100-F260	108.5	9.18	173.28	16.53	138.62	16.53	0.005748
A20-H120-F260	112.65	8.02	172.27	15.41	137.82	15.41	0.006165
A22-H140-F280	123.80	9.30	175.75	15.45	140.60	17.03	0.005596
A22-H160-F280	131.80	9.07	178.35	14.21	142.68	14.21	0.004336
A22-H140-F220	126.50	9.69	174.24	13.94	139.39	13.94	0.004139
A24-H120-F300	116.80	7.47	177.54	15.09	142.03	15.09	0.005892
A24-H150-F260	118.3	8.57	178.41	16.76	142.73	16.76	0.003887
A24-H150-F300	116.3	7.03	190.26	16.63	152.21	16.63	0.005332
IA14-H100-F180	106.1	7.74	155.31	12.63	124.25	12.63	0.003936
IA20-H100-F260	103.41	6.98	152.53	11.37	122.02	11.37	0.005459

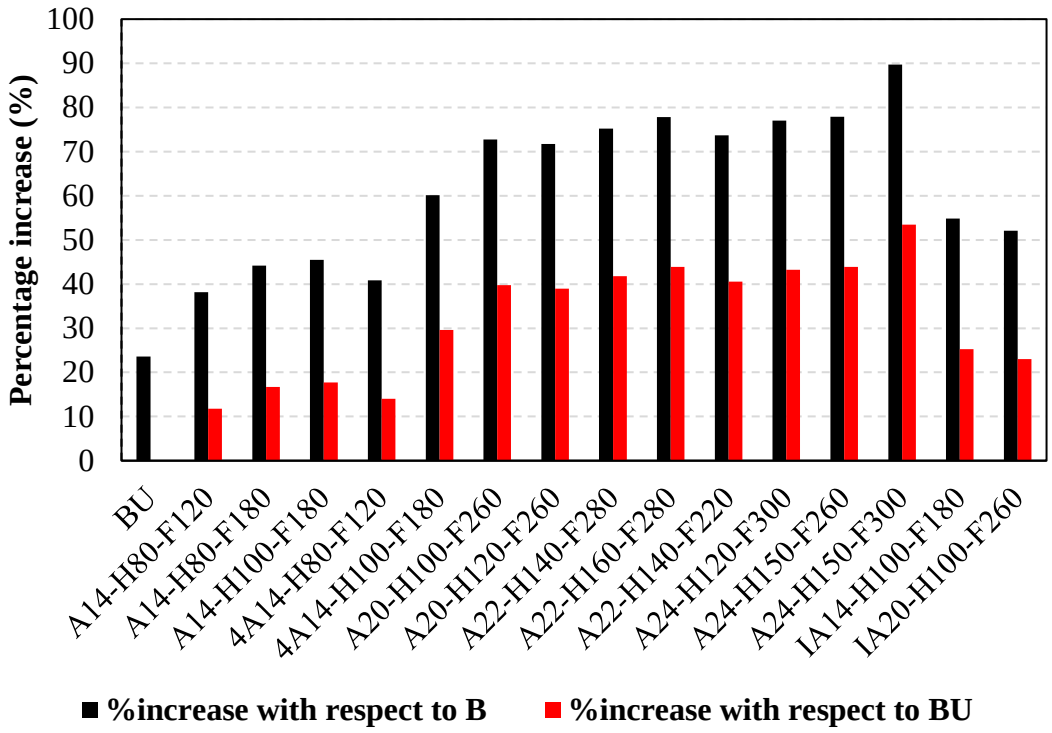

Figure 48: Percentage increase in ultimate load for the tested specimens

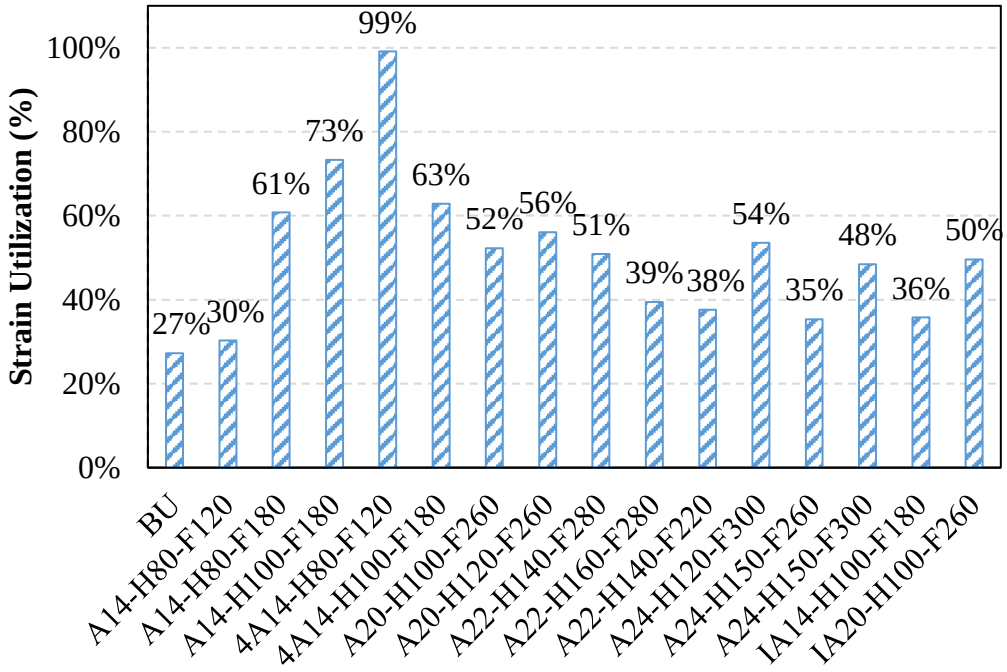

Figure 49: Percentage of strain utilization

5.1.3. Effect of anchor dowel diameter

In this study, four dowel diameters were considered: 14, 20, 22, and 24 mm. The study is intended to investigate the behavior of strengthened RC beams and anchored with large diameter anchors, namely 20 mm and above. The specimens anchored with 14 mm diameter were tested for the purpose of comparison. A conspicuous trend is detected in Fig. 48 where increasing the dowel diameter resulted in an increase in the flexural load carrying capacity. Increasing the dowel diameter from 14 to 20 mm resulted in an average raise in the ultimate load from 46% to 74% compared to the control beam. Beams anchored with 22- and 24-mm diameter anchors averaged a percentage increase of 76% and 82%, respectively. On the contrary, smaller diameter anchors are in favor of larger diameters regarding the degree of strain utilization and the maximum strain attained in the CFRP laminates. This is clearly depicted in Figs. 49. In regard to the performance at failure, there was no clear trend associated with the anchor dowel diameter. Overall, increasing the dowel diameter results in increasing the flexural load-carrying capacity but adversely affects the strain in the CFPR laminates at ultimate loads.

5.1.4. Effect of embedment depth

The effect of anchor's embedment depth on the flexural response of strengthened RC beams was explored in this study. For each dowel diameter, two values of embedment depth were tested. As mentioned earlier, the embedment depth was designed according to the common practices in the field as a value greater than or equal to six times the anchor diameter ($6d_a$). Also, lesser values of embedment depth than the limit were investigated to check if the limit is critical for the development of adequate flexural strength. Therefore, for anchor diameters 14 and 22 mm, two values of the embedment depth were tested, one equals the limit and the other equals to $5d_a$. For anchor diameters of 20 and 24 mm, the two values of embedment depths included one that equals the limit, and the other is equal to $7d_a$. In Fig. 50, the percentage increase in the ultimate load with respect to the control specimen was plotted against the embedment depth where each series was classified according to the dowel diameter. In addition, the results of the percentage increase in load capacity for each embedment depth limit were plotted against the anchor's dowel diameter in Fig. 51. A marginal effect of the embedment depth is observed in three groups (14, 20, and 22). Whereas a

linear increase in the flexural capacity is deducted from Fig. 51 for the beams anchored with anchors of 24 mm diameter when raising the embedment depth from 5da to 6da. Thus, it can be concluded that the anchor's embedment depth has no clear effect on increasing the capacity of strengthened RC beams.

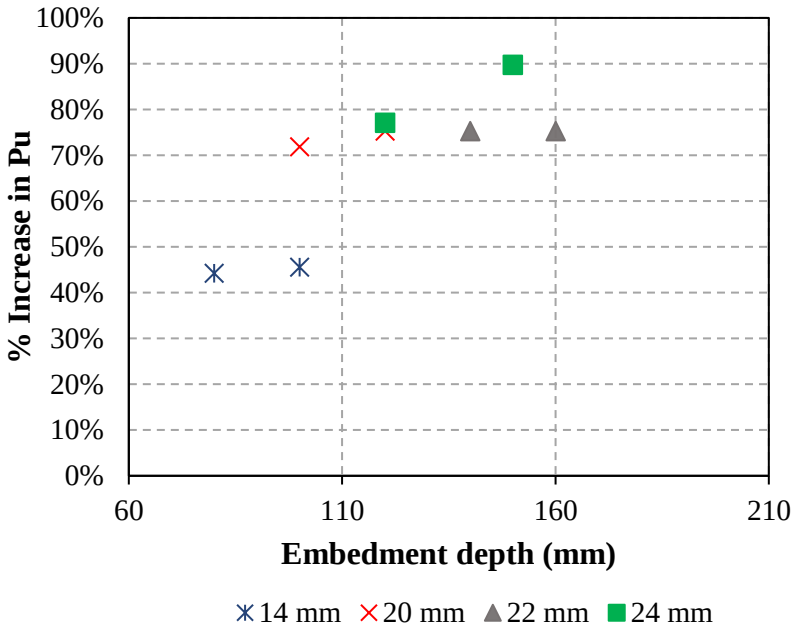

Figure 50: Effect of embedment depth for different groups

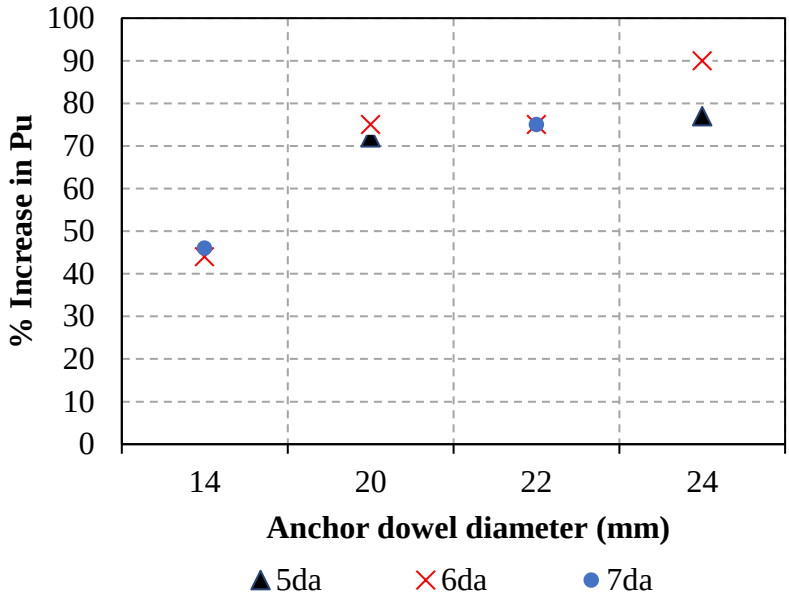

Figure 51: Effect of embedment depth

5.1.5. Effect of fan length

The anchor fan length effect was investigated in this study by varying the fan length for each anchor dowel diameter. Hence, two fan lengths values were tested for anchors with diameter 14, 22, and 24 mm, respectively. It was mentioned previously that there are no available models in the literature that incorporate the fan length. Therefore, ACI440.2R-17 equation of the minimum development length of FRP [48] was conservatively used to calculate the anchor fan lengths. The other investigated value is less than the calculated by 60 mm. Fig. 52 shows the percentage increase in ultimate load versus the fan length. A linear increase is detected between the two values of the fan lengths in two groups. The remaining group (22 mm diameter anchor) showed almost no increase in the ultimate load when the fan length was increased. Moreover, the strain utilization percentage is plotted for both fan lengths values for all diameters in Fig. 53. It can be detected that going below the value calculated by ACI440.2R-17 equation of the minimum development length of FRP results in a decrease in both the ultimate load and the maximum strain utilized by the laminates. Hence, the limit can be considered adequate for the effective development of FRP splay anchors in flexure.

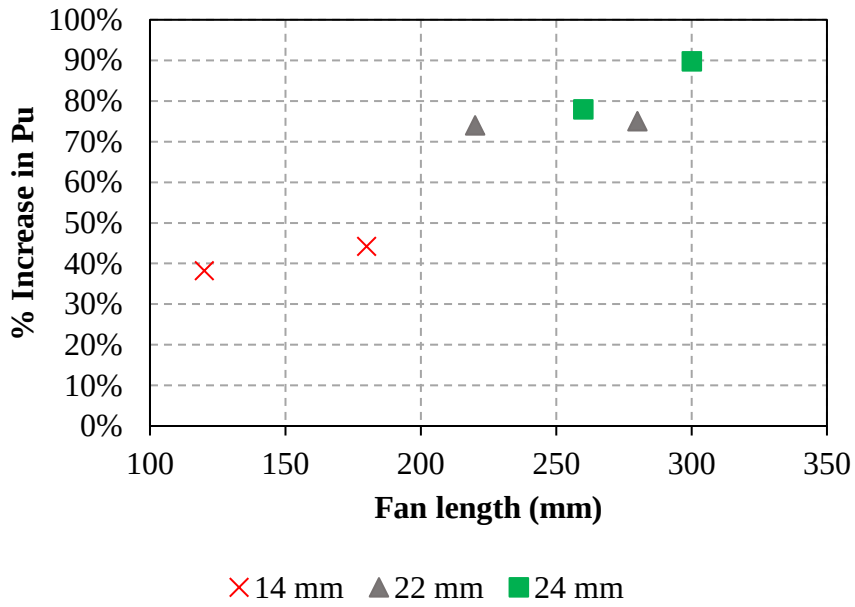

Figure 52: Effect of fan length in different groups

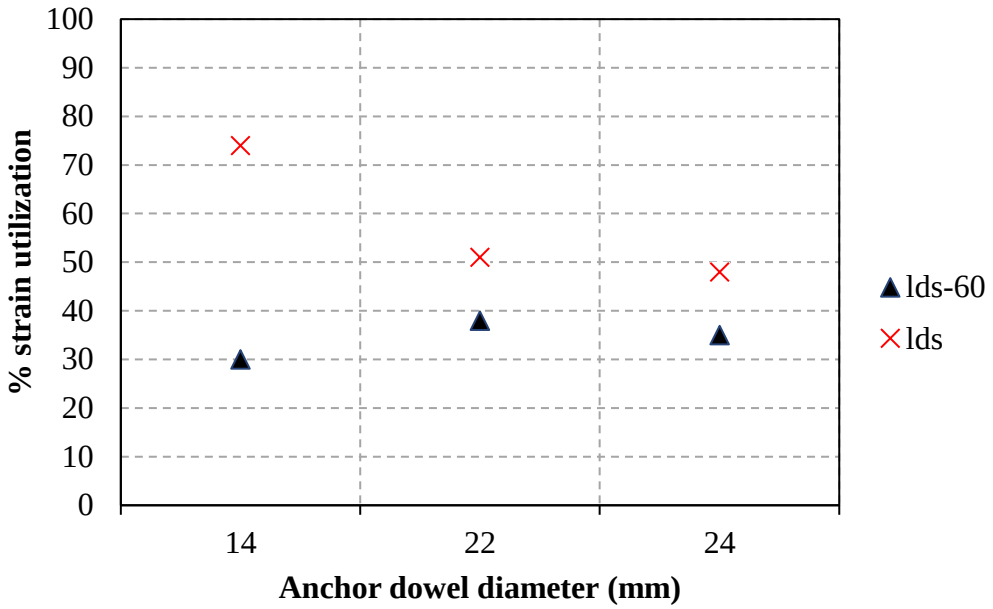

Figure 53: Effect of fan length

5.1.6. Effect of insertion angle

Two strengthened specimens with 45 inclined anchors of diameters 14 and 20 mm were tested and compared to their counterparts that have vertical insertion angles. The comparison is shown in Figs. 54-55. One group showed a higher ultimate load for the inclined anchor compared to the vertical one. However, the failure observed for both of the beams having inclined anchors was unfavorable as mentioned in the failure modes section. An abrupt separation in the concrete cover occurred that was even more brittle than the unanchored beam. Moreover, drilling inclined holes for large-diameter anchors in flexure is impractical since there is a high chance that the drill will be obstructed by a steel bar or a steel stirrup due to inaccuracy in placing the reinforcement during construction. Therefore, it is not recommended to use inclined anchors in strengthened RC beams for flexure.

5.1.7. Effect of the number of anchors

The effect of the number of anchors was explored in this study. Two strengthened beams were anchored with 2 FRP anchors at each end and compared with another two beams having one anchor at each end, with the same diameter, embedment depth, and fan length for each anchor. In terms of the flexural capacity, one beam with 4 anchors showed a superior increase in the ultimate load compared with the rest of the

beams in the group. The other beam having 4 anchors showed an almost similar response to its counterpart. Conversely, this beam had an ultimate strain in the CFRP laminates that is very close to the rupture strain. As shown previously, the behavior of beams with 4 anchors at failure was the most favorable failure behavior among all the tested beams. Overall, it can be concluded that increasing the number of anchors can have a positive effect in controlling the brittle failure of strengthened beams and increasing the utilization of FRP strength.

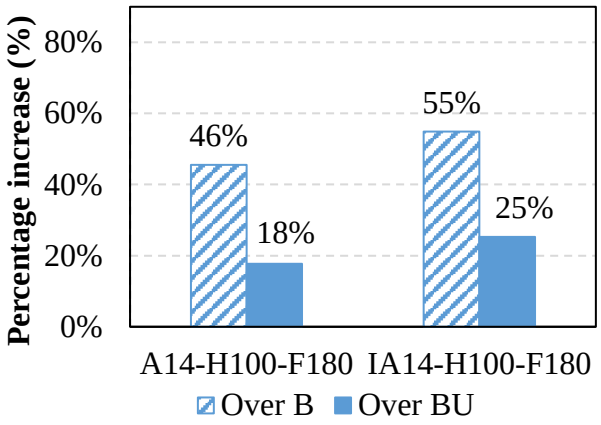

(a) Anchor dowel diameter 14 mm

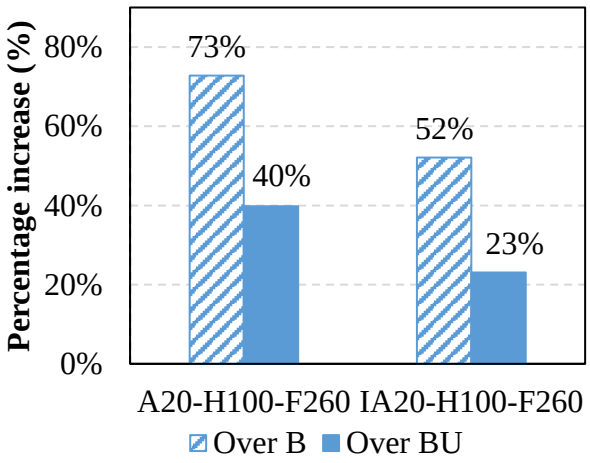

(b) Anchor dowel diameter 20 mm

Figure 54: Effect of insertion angle

5.1.8. Effect of anchor's area to sheet's area ratio (ASR)

The ratio of the anchor's area to the sheet's area (ASR) was examined in this study. In Fig. 55, the percentage increase in the ultimate load was plotted against the ASR value of each specimen. It is observed that beams with the same ASR ratio showed different flexural capacity. Similarly, beams with different ASR exhibited similar ultimate loads. Therefore, it can be deduced that the ASR ratio has no direct influence on the behavior of anchored beams.

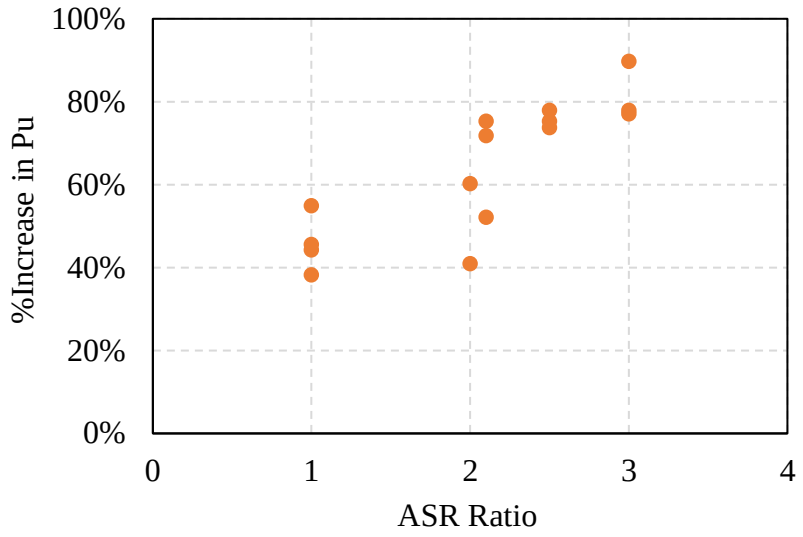

Figure 55: Effect of ASR ratio

5.2. Ductility

The ability of reinforced concrete (RC) beams to deform without breaking or losing strength when subjected to applied loads is referred to as ductility. This characteristic is crucial in structural engineering because it enables RC beams to withstand high levels of strain and stress without breaking. The ductility index, also known as the ratio of the ultimate deformation to the yield deformation (δ_y/δ_u), is frequently used to measure ductility in RC beams. This variable serves as a gauge of the beam's ability to absorb energy during deformation. Because of its role in ensuring that the beam can resist high levels of stress and strain brought on by variables like seismic activity, wind loads, and traffic loads, ductility is a crucial design feature in RC beams. Moreover, ductility enables the beam to experience some deformation prior to failure, providing time for inhabitants of a structure to flee in case of emergency.

Table 7 shows test results in terms of deformation at yield (δ_y), deformation at ultimate load (δ_u), and deformation at final load (δ_f). To further illustrate the comparison, ductility indices were plotted in Fig. 56. Also, the percentage decrease in the ductility index for each specimen with respect to the control beam was calculated and plotted in Fig. 57 It can be observed that the data do not exhibit a discernible trend. For instance, the ductility of larger dowel diameter anchors is comparable to smaller diameter anchors. Moreover, when the embedment depth or fan length was increased for the group of anchors having the same diameter, the ductility slightly increased for some specimens and decreased for others. The group that showed enhanced ductility in comparison with the unanchored specimen (BU) is group 6 (beams anchored with 24 mm diameter anchors). These specimens averaged only a 15.3% decrease compared to BU which showed a 37.5% decrease in the ductility index.

Table 7: Deflection values and ductiltiy results

Group	Designation	δy	δu	δf	μu	%μu
	B	9.88	24.658	29.29	2.50	-
1	BU	6.49	10.12	10.12	1.56	37.5
	A14-H80-F120	10.70	10.70	10.70	1.00	59.9
	A14-H80-F180	6.75	16.76	16.76	2.48	0.5
2	A14-H100-F180	8.67	13.95	13.95	1.61	35.6
	4A14-H80-F120	9.44	16.49	16.49	1.75	30.0
3	4A14-H100-F180	8.77	15.11	15.11	1.72	30.9
	A20-H120-F260	9.18	15.407	15.407	1.92	32.8
4	A20-H100-F260	8.02	16.536	16.536	1.80	17.4
	A22-H140-F280	9.30	15.453	17.034	1.66	33.4
	A22-H160-F280	9.07	14.21	14.21	1.57	37.2
5	A22-H140-F220	9.69	13.941	13.941	1.44	42.4
	A24-H120-F300	7.47	15.09	15.09	2.02	19.1
	A24-H150-F260	8.58	16.76	16.76	1.95	21.7
6	A24-H150-F300	7.03	16.63	16.63	2.37	5.2

	IA14-H100-F180	7.74	12.628	12.628	2.37	34.6
7	IA20-H100-F260	6.98	11.367	11.367	1.63	34.8

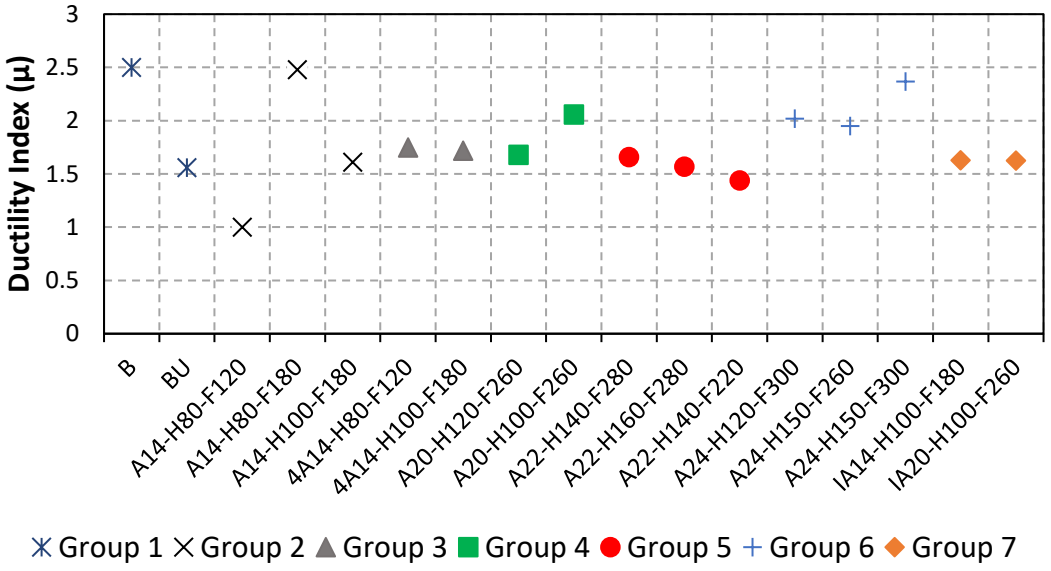

Figure 56: Ductility index for all specimens

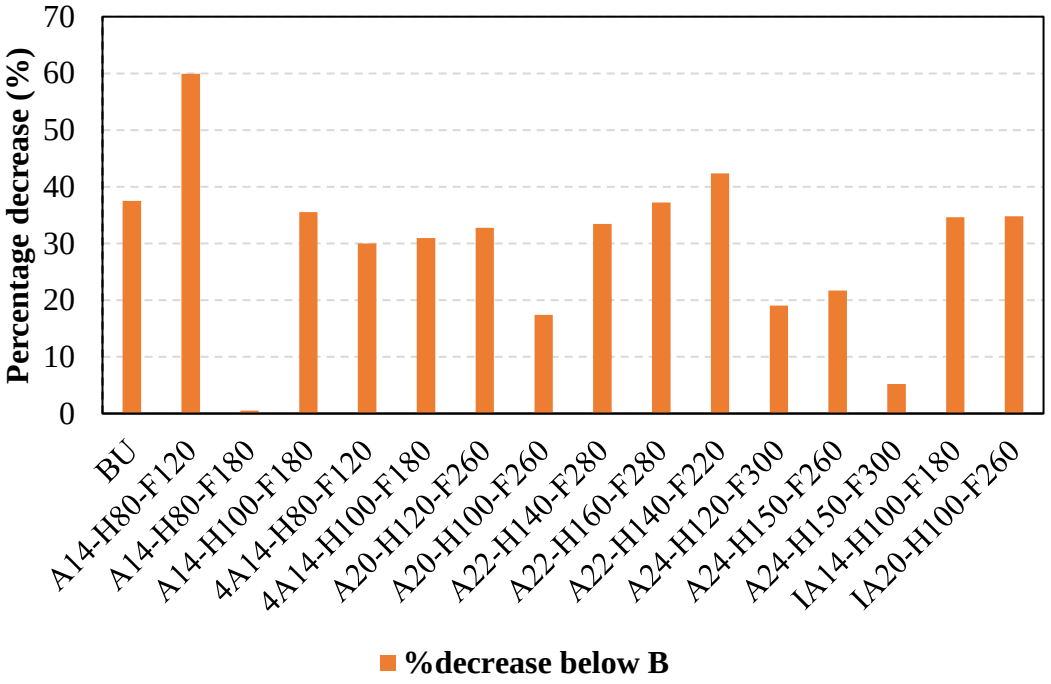

Figure 57: Percentage decrease in ductiltiy index below B

Chapter 6. Analytical Predictions

This chapter presents a comparison of the experimental results with respect to theoretical predictions obtained from current design codes of practice. The first section discusses the flexural strength, and the second section compares the ultimate strain in the CFRP laminates to different proposed models of the debonding strain from design codes and literature.

6.1. Flexural Strength

In this section, the flexural strength was calculated for each tested beam specimen and compared to the experimental ultimate load obtained from the tests. The flexural strength of the unstrengthened control specimen (B) was evaluated in accordance with ACI-318 [55]. Hence, the predicted value of the ultimate flexural load-carrying capacity was found to be 94.54 kN, compared to the experimental value of 100.3 kN. Denoting a 5.7% difference between the experimental and predicted values.

For strengthened specimens, the predicted values of flexural strengths were calculated in accordance with ACI-440.9R-15 [48], *fib*14 [56], and CSA-S806.12 [57]. Since the properties, dimensions, and number of FRP sheets are similar in all specimens, only two values of the predicted flexural strength are calculated from each design code. One is for the strengthened unanchored specimen and the other is for the rest of the anchored specimens because the current design codes do not take into consideration the specific effect of anchors with respect to their design properties. Therefore, the calculation of the flexural strength of anchored specimens was based on the assumption that the strengthened beam will reach the debonding phase. The ratio of the experimental ultimate load to the ($P_{u(Exp)}$) to the predicted ultimate load ($P_{u(Pred)}$) was calculated for each specimen and presented in Table 8. A better illustration of the comparison results is presented in Fig. 58, where $P_{u(exp)}/P_{u(Pred)}$ calculated in accordance with the three codes for each specimen is plotted.

The predictions of CSA code for larger diameters were close to the experimental values. The highest percentage difference among anchored specimens was 20.1% between the predicted and experimental values of the strength.

Table 8: Comparison between predicted and experimental flexural strength

Beam	$P_{u(Exp)}$	$P_{u(exp)}/P_{u(Pred)}$		
		ACI-440 [48]	*fib* 14 [56]	CSA [57]
BU	124.0	1.14	1.06	0.98
A14-H80-F120	138.6	1.27	0.91	0.78
A14-H80-F180	144.6	1.32	0.95	0.82
A14-H100-F180	145.9	1.34	0.96	0.83
4A14-H80-F120	141.3	1.29	0.93	0.80
4A14-H100-F180	160.6	1.47	1.06	0.91
A20-H100-F260	173.3	1.59	1.14	0.98
A20-H120-F260	172.3	1.58	1.13	0.97
A22-H140-F280	175.7	1.61	1.16	0.99
A22-H160-F280	178.4	1.63	1.17	1.01
A22-H140-F220	174.2	1.60	1.15	0.99
A24-H120-F300	177.5	1.63	1.17	1.00
A24-H150-F260	178.4	1.63	1.17	1.01
A24-H150-F300	190.3	1.74	1.25	1.08
IA14-H100-F180	155.3	1.42	1.02	0.88
IA20-H100-F260	152.5	1.40	1.00	0.86

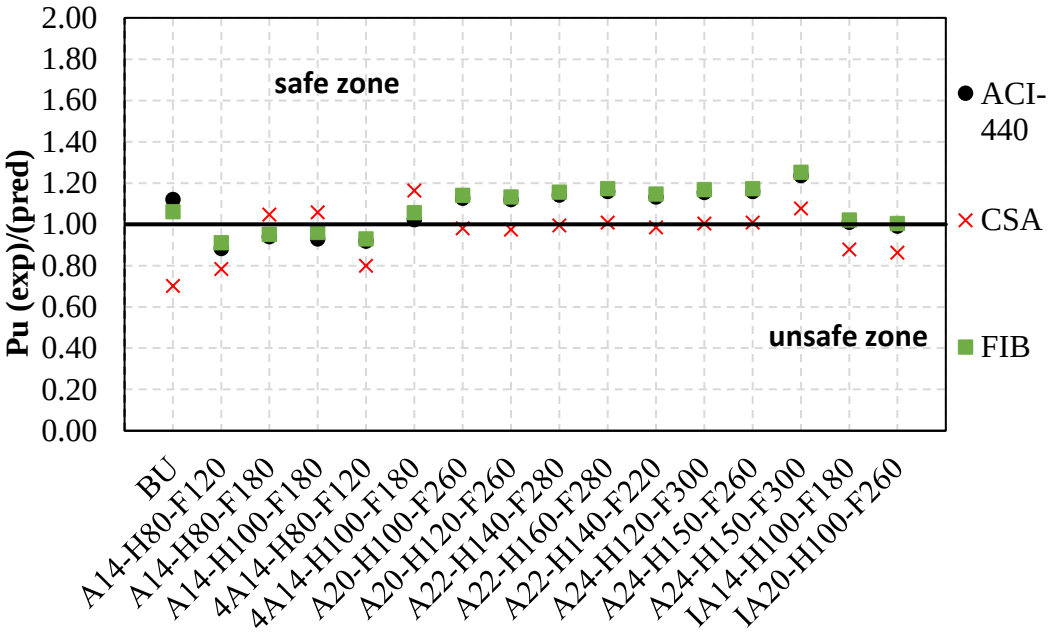

Figure 58: Comparison between the experimental and predicted flexural strength

It can be observed from Fig. 58 that ACI-440 and *fib*14 predictions were very close to each other. For larger diameter anchors (20, 22, and 24 mm), they conservatively predicted the strength of the anchored specimens. The mean value of $P_{u(exp)}/P_{u(Pred)}$ ratio was 1.15 and 1.17 for ACI440, and *fib*14, respectively. In general, ACI440-A and FIB-A provided conservative values of flexural strength for anchored beams. They also underpredicted the strength of the unanchored specimen. A difference of 12.0, and 6.1% is recorded between experimental and predicted ultimate load by ACI440 and *fib*14, respectively.

6.2. Strain in the CFRP laminates at failure

It is widely known that the dominant failure mode of externally bonded FRP laminates strengthening system is the premature debonding of the FRP from concrete. This type of failure prevents the FRP composite from utilizing its ultimate strength. Therefore, FRP rupture strain is rarely reached since the debonding strain at which the FRP sheet is separated from concrete is significantly lower. Hence, design codes specify debonding strain to predict the actual strength that the member would reach when debonding occurs. In this section, the maximum experimentally attained strains in the CFRP laminates for each specimen are compared with predicted strain from the current design codes and models in the literature, as explained in Chapter 3.Table 8 shows the strains calculated in accordance with ACI-440.9R-15 [48], *fib*14 [56], and CSA-S806.12 [57], and two models in the literature: Alsammari & Brena [47], and Zaki et. al. [49]. It should be noted that three different values were calculated for the strain from *fib* 14, since the code distinguishes between debonding strain (FIB-D), strain at delamination (FIB-DEL), and predicted strain in the case of properly anchored laminates (FIB-A). Also, the equation of the debonding strain in Alsammari & Brena [47] is in terms of the anchor's dowel diameter. Therefore, one value was calculated for each anchor depending on its diameter (A14, A20, A22, A24). Fig. 59 illustrates the comparison between predicted and experimental strain values.

Table 9: Calculated strain values from previous models

Design Code/ Model	ε_{deb} (mm/mm)
ACI-440.9R-15 [48]	0.0099
*fib*14 [56], Debonding (FIB-D)	0.00619

*fib*14 [56], Delamination (FIB-DEL)	0.005574
*fib*14 [56], Anchored laminates (FIB-A)	0.009958
CSA-S806.12 [57]	0.007
Alsammari & Brena [47]	A14: 0.01034 A20: 0.01043 A22: 0.01045 A24: 0.01048
Zaki et. al. [49].	0.01099

It can be observed from Fig. 59 that ACI-440 provided close predictions only for two beams out of the 15 anchored specimens. The ratios of the ultimate strain to the predicted debonding strain ($\varepsilon_{ult}/\varepsilon_{deb}$) were as close as 0.93 and 1.25 for beams A14-H100-F180, and 4A14-H80-H120, respectively. The ratio for the rest of the specimens ranged between 0.38 to 0.8. Indicating that the predicted strain is much higher than the actual strain that could be reached in the CFRP laminates. On the contrary, *fib*14 equation for debonding strain is found to be less than the ultimate strain in 8 specimens, with an average of the ratio ($\varepsilon_{ult}/\varepsilon_{deb}$) to be 1.245. Since the majority of the specimens failed by delamination, *fib*14 equation for delamination provided more accurate results. The lowest $\varepsilon_{ult}/\varepsilon_{deb}$ was recorded for specimen A14-H80-F120, which was 0.6. The highest value for $\varepsilon_{ult}/\varepsilon_{deb}$ corresponded to specimen 4A14-H80-H120, which was 1.96. The average value of predicted $\varepsilon_{ult}/\varepsilon_{deb}$ for all of the anchored specimens was 1.002. This indicates that *fib*14 equation for delamination (FIB-DEL) provided close predictions to the actual obtained strain in the CFRP laminate. However, *fib*14 predictions for the debonding strain of properly anchored laminates (FIB-A) are significantly higher than the strain in the majority of specimens. Indicating that this value is overestimated and there should be further investigation into the prediction of this value. Other models from the literature showed overestimated values of the ultimate strain, especially for larger diameter anchors (20,22, and 24 mm). The mean value of $\varepsilon_{ult}/\varepsilon_{deb}$ for larger diameters is found to be 0.561 and 0.534 according to Al sammari and Brena [52], and Zaki et al. [54], respectively.

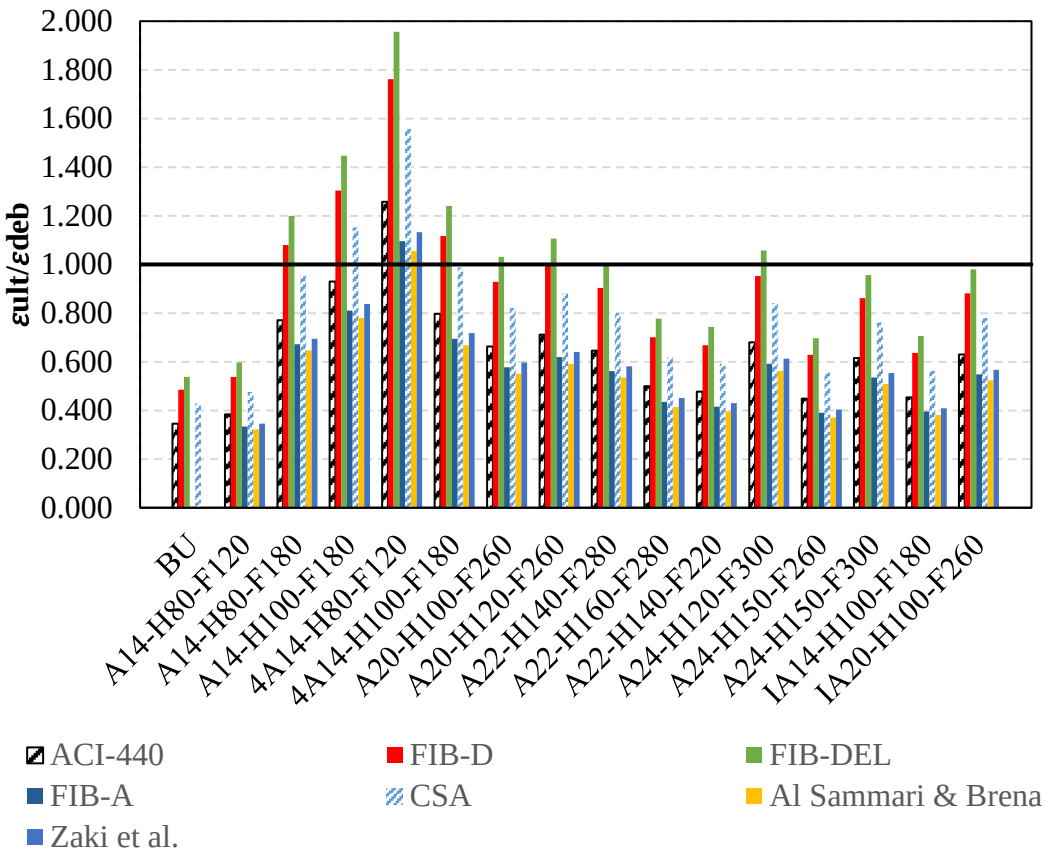

Figure 59: Comparison of ultimate strain to calculated debonding strain from previous models

In Fig. 60 (a-e), the ratio of the ultimate strain to the debonding strain ($\varepsilon ult/\varepsilon deb$) calculated by design codes mentioned above is plotted according to each group separately. It can be deduced that *fib*14 provided close predictions of the ultimate strain in the CFRP laminate for large-diameter anchors. Whereas ACI-440 and CSI overestimated the ultimate strain at which debonding/delamination strain takes place. Moreover, the predictions calculated by the codes herein are for unanchored laminates (except for FIB-A, as mentioned previously). Given that the ratio of the actual ultimate strain to the predicted debonding strains for most of the specimens were below 1, the anchors did not enhance the strain at which the laminate detaches from concrete. However, it improved the strength and the overall behavior of the strengthened beams. Moreover, it is noticed that specimens with larger fan length anchors showed slightly

higher $\varepsilon_{ult}/\varepsilon_{deb}$ values which emphasizes on the effect of having adequate anchor's fan length.

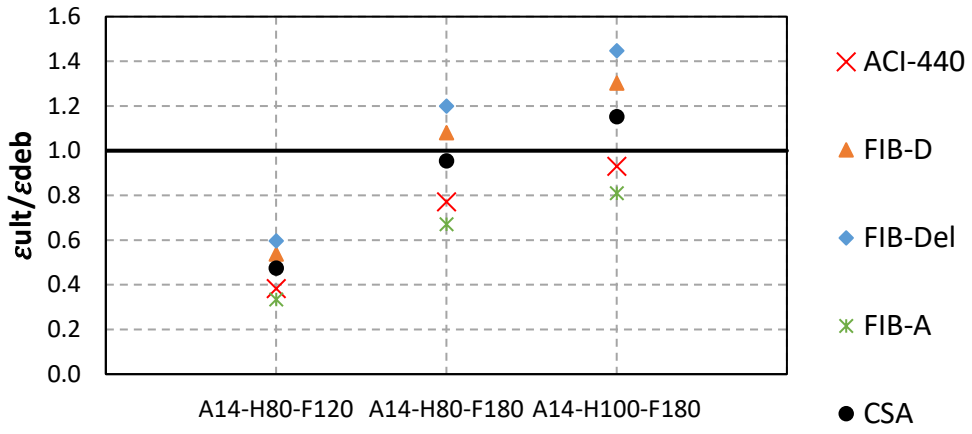

(a) $\varepsilon_{ult}/\varepsilon_{deb}$ for 14-mm anchors

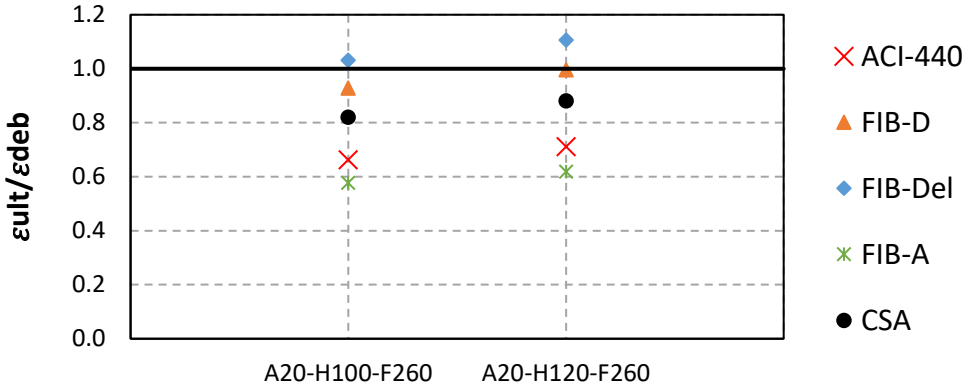

(b) $\varepsilon_{ult}/\varepsilon_{deb}$ for 20-mm anchors

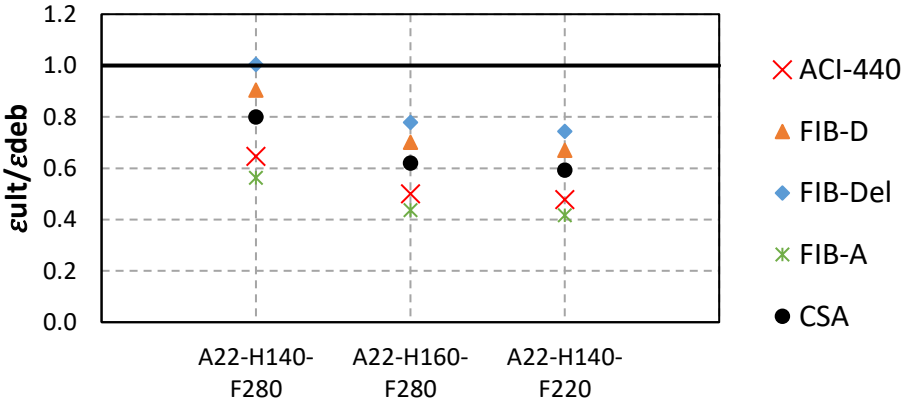

(c) $\varepsilon_{ult}/\varepsilon_{deb}$ for 22-mm anchors

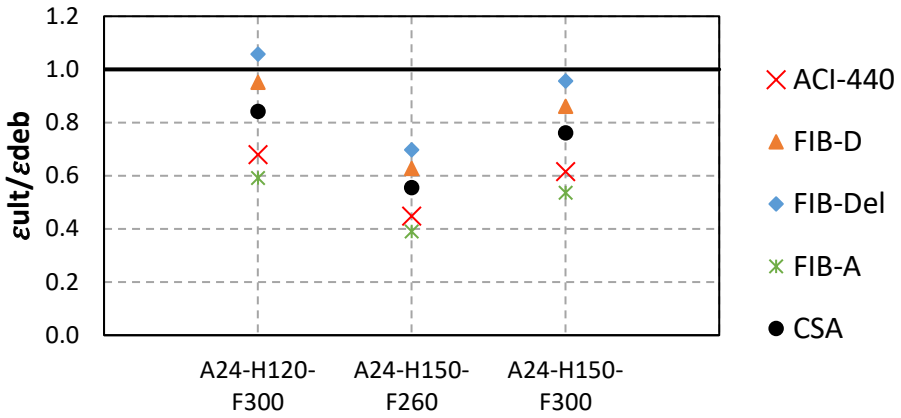

(d) $\varepsilon_{ult}/\varepsilon_{deb}$ for 24-mm anchors

Figure 60: Comparison of $\varepsilon_{ult}/\varepsilon_{deb}$ from different codes according to the diameter

Chapter 7. Summary and Conclusions

7.1. Summary

Fiber-reinforced polymers (FRP) have a proven strength enhancement capability when installed into Reinforced Concrete (RC) beams. However, the load-carrying capacity of strengthening systems is largely sacrificed due to the brittle failure associated with FRP composites. The use of carbon fiber-reinforced polymers (CFRP) splay anchors was proposed to mitigate debonding and enhance the capacity of strengthened beams. Research related to the design parameters of CFRP splay anchors has been widely active in the past few years. However, few studies were directed towards the flexural behavior of RC beams anchored with large CFRP splay anchors, specifically, anchors with a diameter of more than 14 mm. Further, the use of FRP anchors in rehabilitation projects is still limited due to the lack of guidance on their design in the existing guidelines. To bridge this research gap, a total of seventeen beams were cast and externally strengthened with CFRP laminates in flexure. Fifteen beams were anchored with anchored with different configurations of CFRP splay anchors. The parameters investigated in this study are anchor's embedment depth, fan length, number of anchors, and insertion angle. Four-point bending test was performed on all specimens. The behavior of the specimens in terms of load-deflection, flexural strength, strain in the CFRP laminates, and ductility of the specimens was studied and discussed. Furthermore, the flexural strength and expected debonding strain were predicted using current design codes of practice, namely ACI-440.9R-15 [48], *fib*14 [56], and CSA-S806.12 [57], and two models in the literature: Alsammari & Brena [47], and Zaki et. al. [49].

7.2. Conclusions

The study's primary conclusions are based on the experimental findings and theoretical predictions, and they are as follows:

1. The anchorage of CFRP laminates with CFRP splay anchors positively affected the flexural capacity of the specimens. It increased the load-carrying capacity in the range of 38-90% compared to a control

unstrengthened specimen and 12-53% compared to unanchored strengthened specimen, respectively.

2. The mode of failure in the majority of specimens was delamination/concrete cover separation. The use of CFRP anchors delayed the delamination and improved the behavior of the beams at failure.
3. The effective strain in the CFRP laminates was increased by CFRP splay anchors. The average percentage of strain utilization in anchored beams was 51% compared to 27% strain utilization in the unanchored beam. The percentage of strain utilization in anchored specimen ranged from 30% to 99%.
4. Increasing the dowel diameter resulted in an increase in the flexural load carrying capacity. The percentage increase in the flexural strength of beams anchored with larger diameter (20, 22, and 24 mm) ranged between 74-82% compared to an average of 46% exhibited by the beams anchored with 14 mm diameter anchors.
5. The anchor's embedment depth had a marginal effect on the flexural strength of anchored specimens. The investigated embedment depth values were $5d_a$, $6d_a$, and $7d_a$ where d_a is the anchor's dowel diameter.
6. ACI440.2R-17 equation of the minimum development length of FRP can be considered adequate for the effective development of FRP splay anchors in flexure. Going below the value calculated by ACI440.2R-17 equation results in a decrease in both the ultimate load and the maximum strain utilized by the laminates.
7. The failure observed in specimens having inclined anchors was unfavorable. An abrupt separation in the concrete cover occurred that was even more brittle than the unanchored beam. Moreover, drilling inclined holes for large-diameter anchors in flexure is impractical since there is a high chance that the drill will be obstructed by a steel bar or a steel stirrup due to inaccuracy in placing the reinforcement during construction. Therefore, it is not recommended to use inclined anchors in strengthened RC beams for flexure.

8. Increasing the number of anchors has a positive effect on controlling the brittle failure of strengthened beams and increasing the utilization of FRP strength.
9. The percentage decrease in the ductility index of most of the anchored specimens compared to the control beam was comparable to the unanchored beam. However, some of the specimens showed improved ductility.
10. The mean value of the experimental to predicted ultimate load ratio was 1.15 and 1.17 according to ACI440, and *fib*14 guidelines for strengthened (unanchored) beams, respectively. In general, ACI440 and *fib*14 provided conservative values of flexural strength for anchored beams. They also conservatively predicted the strength of the unanchored specimen. A difference of 12.0, and 6.1% is recorded between experimental and predicted ultimate load by ACI440 and *fib*14.

7.3. Suggested Future Research work

The following proposed topics could be addressed in future research:

- Examining a wider range of parameters that affect the effectiveness of FRP splay anchors on the flexural strength of strengthened RC beams.
- Investigating more values of the design parameters of FRP splay anchors to develop design equations that include the contribution of anchorage.
- Studying the behavior of anchored strengthened specimens under different loading conditions, namely, seismic, fatigue, and severe environmental conditions.
- Develop accurate models that include the effect of anchorage on strain utilization and flexural strength enhancement.

References

[1] Y. H. Mugahed Amran, R. Alyousef, R. S. M. Rashid, H. Alabduljabbar, and C. C. Hung, “Properties and applications of FRP in strengthening RC structures: A review,” Structures, vol. 16, pp. 208–238, Nov. 2018.

[2] M. N. Danraka, H. Mahir Mahmod, and O.-K. J. Oluwatosin, “Strengthening of Reinforced Concrete Beams using FRP Technique: A Review,” International Journal of Engineering Science and Computing, vol. 7, pp. 13199-13213 Jun. 2017.

[3] H. A. Rasheed, *Strengthening Design of Reinforced Concrete with FRP*. Boca Raton: CRC Press, 2014, pp. 53-65.

[4] A. Siddika, M. A. al Mamun, R. Alyousef, and Y. H. M. Amran, “Strengthening of reinforced concrete beams by using fiber-reinforced polymer composites: A review,” *Journal of Building Engineering*, vol. 25, article 100798, Sep. 2019.

[5] J. Dong, Q. Wang, and Z. Guan, “Structural behaviour of RC beams with external flexural and flexural-shear strengthening by FRP sheets,” Compos B Eng, vol. 44, no. 1, pp. 604–612, Jan. 2013.

[6] R. Kotynia, Hussien, A. Baky, K. W. Neale, M. Asce, and U. A. Ebead, “Flexural Strengthening of RC Beams with Externally Bonded CFRP Systems: Test Results and 3D Nonlinear FE Analysis”, J. Compos. Constr., vol. 12, no. 2, pp. 190-201, 2008.

[7] S. T. Smith and J. G. Teng, “FRP-strengthened RC beams. I: review of debonding strength models,” *Engineering Structures*, vol. 24, pp. 385-395, 2002.

[8] G. M. Chen, J. G. Teng, J. F. Chen, and Q. G. Xiao, “Finite element modeling of debonding failures in FRP-strengthened RC beams: A dynamic approach,” *Comput Struct*, vol. 158, pp. 167–183, Jun. 2015.

[9] M. Arduini, A. Di Tommaso, and A. Nanni, “Brittle Failure in FRP Plate and Sheet Bonded Beams,” ACI Struct J, vol. 94, pp. 363–370, 1997.

[10] H. Akbarzadeh Bengar and A. A. Shahmansouri, “A new anchorage system for CFRP strips in externally strengthened RC continuous beams,” *Journal of Building Engineering*, vol. 30, Jul. 2020.

[11] J. Esmaeili, O. R. Aghdam, K. Andalibi, J. Kasaei, and O. Gencel, “Experimental and numerical investigations on a novel plate anchorage system to solve FRP debonding problem in the strengthened RC beams,” *Journal of Building Engineering*, vol. 45, Jan. 2022.

[12] A. Mostafa and A. G. Razaqpur, “CFRP Anchor for Preventing Premature Debonding of Externally Bonded FRP Laminates from Concrete,” *Journal of Composites for Construction*, vol. 17, no. 5, pp. 641–650, Oct. 2013.

[13] R. Kalfat and R. Al-Mahaidi, “Improvement of FRP-to-concrete bond performance using bidirectional fiber patch anchors combined with FRP spike anchors,” *Compos Struct*, vol. 155, pp. 89–98, Nov. 2016.

[14] E. del Rey Castillo, D. Dizhur, M. Griffith, and J. Ingham, “Strengthening RC structures using FRP spike anchors in combination with EBR systems,” *Compos Struct*, vol. 209, pp. 668–685, Feb. 2019.

[15] S. V. Grelle. “Categorization and experimental evaluation of anchorage systems for fiber-reinforced polymer laminates bonded to reinforced concrete structures.” M.A Thesis, Missouri University of Science and Technology, United States, 2011.

[16] S. v. Grelle and L. H. Sneed, “Review of Anchorage Systems for Externally Bonded FRP Laminates,” *International Journal of Concrete Structures and Materials*, vol. 7, no. 1. Korea Concrete Institute, pp. 17–33, Mar. 01, 2013.

[17] A. K. Al-Tamimi, R. Hawileh, J. Abdalla, and H. A. Rasheed, “Effects of Ratio of CFRP Plate Length to Shear Span and End Anchorage on Flexural Behavior of SCC RC Beams,” *Journal of Composites for Construction*, vol. 15, no. 6, pp. 908–919, Dec. 2011.

[18] O. R. Abuodeh, R. A. Hawileh, and J. A. Abdalla, “Nonlinear finite element models of reinforced concrete beams strengthened in bending with mechanically fastened aluminum alloy plates,” *Comput Struct*, vol. 253, Sep. 2021.

[19] E. del Rey Castillo, R. Kanitkar, S. T. Smith, M. C. Griffith, and J. M. Ingham, “Design approach for FRP spike anchors in FRP-strengthened RC structures,” *Compos Struct*, vol. 214, pp. 23–33, Apr. 2019.

[20] S. Kim and S. Smith, “Behaviour of Handmade FRP Anchors under Tensile Load in Uncracked Concrete.” *Advances in Structural Engineering*, vol. 12, no. 6, 2009.

[21] H. H. Mhanna, R. A. Hawileh, J. A. Abdalla, A. S. D. Salama, and T. Alkhrdaji, “Shear Strengthening of Reinforced Concrete T-Beams with Anchored CFRP Laminates,” *Journal of Composites for Construction*, vol. 25, no. 4, p. 04021030, Aug. 2021.

[22] E. del Rey Castillo, D. Dizhur, M. Griffith, and J. Ingham, “Experimental testing and design model for bent FRP anchors exhibiting fiber rupture failure mode,” *Compos Struct*, vol. 210, pp. 618–627, Feb. 2019.

[23] W. Sun, H. Liu, Y. Wang, and T. He, “Impacts of configurations on the strength of FRP anchors,” *Compos Struct*, vol. 194, pp. 126–135, Jun. 2018.

[24] P. Villanueva Llauradó, T. Ibell, J. Fernández Gómez, and F. J. González Ramos, “Pull-out and shear-strength models for FRP spike anchors,” *Compos B Eng*, vol. 116, pp. 239–252, May 2017.

[25] H. Zhang, S. T. Smith, R. J. Gravina, and Z. Wang, “Modelling of FRP-concrete bonded interfaces containing FRP anchors,” *Constr Build Mater*, vol. 139, pp. 394–402, May 2017.

[26] W. Sun, “Development of a testing methodology for the design and quality control of carbon fiber reinforced polymer (CFRP) anchors,” *Constr Build Mater*, vol. 164, pp. 150–163, Mar. 2018.

[27] D. M. J. C. Allen Ross Joseph W. Tedesco and Mary L. Hughes, “Strengthening of Reinforced Concrete Beams with Externally Bonded Composite Laminates,” *ACI Struct J*, vol. 96, no. 2, 1999.

[28] M. A. and A. Nanni, “Parametric Study of Beams with Externally Bonded FRP Reinforcement,” *ACI Struct J*, vol. 94, no. 5, 1997.

[29] S. F. Breña, R. M. Bramblett, S. L. Wood, and M. E. Kreger, “Increasing flexural capacity of reinforced concrete beams using carbon fiber-reinforced polymer composites,” *ACI Struct J*, vol. 100, pp. 36–46, Jun. 2003.

[30] G. Spadea, F Bencardino, and R. N. Swamy, “Structural Behavior of Composite RC Beams with Externally Bonded CFRP.” *J. Compos. Constr*, vol. 2, no. 3, pp. 132-137, 1998.

[31] Y. T. Obaidat, S. Heyden, O. Dahlblom, G. Abu-Farsakh, and Y. Abdel-Jawad, “Retrofitting of reinforced concrete beams using composite laminates,” *Construction and Building Materials*, vol. 25, no. 2. pp. 591–597, Feb. 2011.

[32] Z. Wu, W. Li, and N. Sakuma, “Innovative externally bonded FRP/concrete hybrid flexural members,” *Compos Struct*, vol. 72, no. 3, pp. 289–300, Mar. 2006.

[33] D. Chen, G. Sun, M. Meng, X. Jin, and Q. Li, “Flexural performance and cost efficiency of carbon/basalt/glass hybrid FRP composite laminates,” *Thin-Walled Structures*, vol. 142, pp. 516–531, Sep. 2019.

[34] J. A. Abdalla, A. Mohammed, and R. A. Hawileh, “Flexural strengthening of reinforced concrete beams with externally bonded hybrid systems,” in *Procedia Structural Integrity*, 2020, vol. 28, pp. 2312–2319.

[35] N. Attari, S. Amziane, and M. Chemrouk, “Flexural strengthening of concrete beams using CFRP, GFRP and hybrid FRP sheets,” *Constr Build Mater*, vol. 37, pp. 746–757, Dec. 2012.

[36] D. Chen, G. Sun, M. Meng, X. Jin, and Q. Li, “Flexural performance and cost efficiency of carbon/basalt/glass hybrid FRP composite laminates,” *Thin-Walled Structures*, vol. 142, pp. 516–531, Sep. 2019.

[37] L. Bizindavyi and K. W. Neale, “Transfer Lengths and Bond Strengths for Composites Bonded to Concrete,” *J. Compos. Constr*, vol. 3, no. 4, pp. 153-160, 1999.

[38] A. T. Al-Sammari and S. F. Breña, “Strength of Carbon Fiber-Reinforced Polymer (CFRP) sheets bonded to concrete with CFRP spike anchors,” *ACI Struct J*, vol. 118, no. 1, pp. 153–166, Jan. 2021.

[39] J. G. Teng, J. F. Chen, and S. T. Smith, “Debonding failures in FRP-strengthened RC beams: Failure modes, existing research and future challenges,” in Proc. *Composites in Construction: A reality*, 2001, pp. 139–148.

[40] J. G. Teng, S. T. Smith, J. Yao, and J. F. Chen, “Intermediate crack-induced debonding in RC beams and slabs,” in Proc. *Construction and Building Materials*, Sep. 2003, vol. 17, no. 6–7, pp. 447–462.

[41] B. Yalim, A. Serhat Kalayci, and A. Mirmiran, “Performance of FRP-Strengthened RC Beams with Different Concrete Surface Profiles”, *J. Compos. Constr*, vol. 12, no. 6, pp. 626-534, 2008.

[42] T. Ozbakkaloglu and M. Saatcioglu, “Tensile Behavior of FRP Anchors in Concrete”, *Journal of Composites for Construction*, vol. 13, no. 2, pp. 82–92, 2009.

[43] G. Özdemir, “Mechanical Properties of CFRP Anchorages.” M.A. thesis, Middle East Technical University, Turkey, 2005.

[44] S. Jin Kim and S. T. Smith, “Pullout Strength Models for FRP Anchors in Uncracked Concrete,” *Journal of Composites for Construction*, vol. 14, no. 4, pp. 406–414, 2010.

[45] T. Ozbakkaloglu, C. Fang, and A. Gholampour, “Influence of FRP anchor configuration on the behavior of FRP plates externally bonded on concrete members,” *Eng Struct*, vol. 133, pp. 133–150, Feb. 2017.

[46] I. A. Cortez Flores, J. Fernández Gómez, P. Villanueva Llauradó, and A. Ferreira, “An empirical model to estimate FRP anchored joint strength using spike anchors,” *Compos Struct*, vol. 254, Dec. 2020.

[47] A. T. Al-Sammari and S. F. Breña, “Strength of Carbon Fiber-Reinforced Polymer (CFRP) sheets bonded to concrete with CFRP spike anchors,” *ACI Struct J*, vol. 118, no. 1, pp. 153–166, Jan. 2021.

[48] ACI Committee 440, “Guide for the design and construction of externally bonded FRP systems for strengthening concrete structures (ACI 440. 2R- 17),” American Concrete Institute, Farmington Hills (MI), 2017.

[49] M. A. Zaki, H. A. Rasheed, and T. Alkhrdaji, “Performance of CFRP-strengthened concrete beams fastened with distributed CFRP dowel and fiber anchors,” *Compos B Eng*, vol. 176, Nov. 2019.

[50] W. Sun, S. Liu, and C. Zhang, “An effective improvement for enhancing the strength and feasibility of FRP spike anchors,” *Compos Struct*, vol. 247, Sep. 2020.

[51] W. A. Shekarchi, D. K. Pudleiner, N. K. Alotaibi, W. M. Ghannoum, and J. O. Jirsa, “Carbon fiber-reinforced polymer spike anchor design recommendations,” *ACI Struct J*, vol. 117, no. 6, pp. 171–182, Nov. 2020.

[52] W. Sun. “Behavior of Carbon Fiber Reinforced Polymer (CFRP) Anchors Strengthening Reinforced Concrete Structures.” PhD, The University of Texas at Austin, United States, 2014.

[53] D. Pudleiner, “Design considerations based on size effects of anchored carbon fiber reinforced polymer (CFRP) systems.” M.A. thesis, The University of Texas at Austin, United States, 2016.

[54] “ASTM A370-18, “Standard Test Methods and Definitions for Mechanical Testing of Steel Products,” ASTM International, West Conshohocken, PA, 2018.

[55] ACI Committee 318, "ACI 318-19 Building Code Requirements for Structural Concrete," American Concrete Institute, Farmington Hills (MI), 2019.

[56] *fib* Bulletin No. 14, “Externally bonded FRP reinforcement for RC structures,” Technical Report, Federation International Du Béton, France, 2001.

[57] Canadian Standards Association, “Design and construction of building structures with fibre-reinforced polymers (CSA-S806.12(R2017)),” *Canadian Standards Association*, Mississauga, Ontario, 2017.

Vita

Maha Ahmad Assad was born in 1995, in Ramallah, Palestine. She received her primary and secondary education in Ramallah, Palestine. She graduated from high school in 2013 among the top 10 students in Ramallah District. She was awarded the Palestinian government scholarship to study Bachelors in Birzeit University. She received her B.Sc. degree with distinction in Civil Engineering from Birzeit University in 2018. From 2018 to 2021, she worked as a teaching assistant in the same university.

In September 2020, she joined the Civil Engineering master's program in the American University of Sharjah as a graduate teaching assistant. During her master's study, she co-authored one journal paper and 3 conference papers which were presented in local and international conferences.